Soft Matter

PAPER

View Article Online
View Journal | View Issue

Cite this: *Soft Matter*, 2022, **18**, 3531

The morphological role of ligand inhibitors in blocking receptor- and clathrin-mediated endocytosis†

Daniele Agostinelli,[ab] Gwynn J. Elfring[ab] and Mattia Bacca*[abc]

Cells often internalize particles through endocytic pathways that involve the binding between cell receptors and particle ligands, which drives the cell membrane to wrap the particle into a delivery vesicle. Previous findings showed that receptor-mediated endocytosis is impossible for spherical particles smaller than a minimum size because of the energy barrier created by membrane bending. In this study, we investigate the morphological role of ligand inhibitors in blocking endocytosis, inspired by antibodies that inhibit virus ligands to prevent infection. While ligand inhibitors have the obvious effect of reducing the driving force due to adhesion, they also have a nontrivial (morphological) impact on the entropic and elastic energy of the system. We determine the necessary conditions for endocytosis by considering the additional energy barrier due to the membrane bending to wrap the inhibiting protrusions. We find that inhibitors increase the minimum radius previously reported, depending on their density and size. In addition, we extend this result to the case of clathrin-mediated endocytosis, which is the most common pathway for virus entry. The assembly of a clathrin coat with a spontaneous curvature increases the energy barrier and sets a maximum particle size (in agreement with experimental observations on spherical particles). Our investigation suggests that morphological considerations can inform the optimal design of neutralizing viral antibodies and new strategies for targeted nanomedicine.

Received 2nd December 2021,
Accepted 28th March 2022

DOI: 10.1039/d1sm01710a

rsc.li/soft-matter-journal

1 Introduction

Endocytosis is a fundamental process by which cells uptake external particles. This can occur through different pathways.[1,2] One observed mechanism exploits the binding affinity between cell receptors and particle ligands, leading the cell membrane to wrap the whole particle into a delivery vesicle. The wrapping process can involve also proteins – present in the cytoplasm – which form a coated vesicle having spontaneous curvature, thereby facilitating the internalization of particles with selected size.[3]

Cells commonly use endocytosis to internalize nutrients, but the process can also result in undesired viral entry and hence the infection of the cell. A physical description of endocytosis is thus crucial for understanding nutrient uptake, viral infection, and nanoparticle engineering for diagnostics and targeted therapies requiring a selective uptake. The last few decades saw significant progress towards a fundamental understanding of some entry mechanisms, with much focus on applications in the context of nanomedicine.[4–9] A continuously growing body of literature supports the view that cell entry depends on multiple factors, such as particle shape, size, surface chemistry, surface topology, and mechanical properties.[2,10,11]

Nanoparticle size has long been recognized to determine the fate of endocytosis.[2,11,12] Theoretical results predict that spherical particles can enter cells *via* receptor-mediated endocytosis only if their size is within a certain range. For a single particle, the minimum radius results from the competition between the enthalpic gain of receptor–ligand bonds and the cost of membrane bending and receptor relocation, whereas the maximum radius is due to a shortage of cell receptors.[13] In the case of particle–particle interactions, attractive forces lower the minimum radius[14] whereas repulsive ones increase it.[15] Experimental observations also find a size-dependent uptake of nanoparticles with optimal diameter of about 50 nm, in different settings (particle materials and cells) and with various approaches, such as using flow cytometry to measure the intensity of nanoparticle markers or measuring the uptake force *via* atomic force microscopy cantilever.[16–19] Experimental studies show a similar size-dependent uptake of nanoparticles

[a] *Mechanical Engineering Department, University of British Columbia, Vancouver, BC V6T 1Z4, Canada*
[b] *Institute of Applied Mathematics, University of British Columbia, Vancouver, BC V6T 1Z4, Canada. E-mail: mbacca@mech.ubc.ca*
[c] *School of Biomedical Engineering, University of British Columbia, Vancouver, BC V6T 1Z4, Canada*

† A preliminary version of this work, 10.1101/2021.10.01.462837, was deposited in bioRxiv on October 02, 2021.

via clathrin-mediated endocytosis,[20–23] which is the most common entry process of viruses.[24,25]

Nanoparticle shape is another crucial factor for cell entry, as suggested by the fact that viruses, for example, are highly variable in both size and shape. Theoretical analyses show that the entry of ellipsoidal particles depends on their aspect ratio, with endocytosis occurring only within a certain range of values.[26] Moreover, one-dimensional nanomaterials might enter perpendicular or parallel to the membrane, depending on the ratio between membrane tension and bending stiffness.[27] This is consistent with recent coarse-grained molecular dynamics simulations that show different shapes (oblate and prolate ellipsoids, cubes, spheres, discs and rods) have different wrapping efficiencies according to the entry mode.[28] Some experiments also find this shape-dependence: spherical gold nanoparticles are internalized more efficiently than rod-shaped nanoparticles with aspect ratios 1 : 3 and 1 : 5,[17] and the uptake of carbon nanotubes follows a bell-shaped function of the tube length.[29]

Recent research has also addressed the role of the mechanical properties of nanoparticles in the wrapping process. For example, theoretical studies suggested that wrapping is more efficient for rigid particles than for soft particles, due to their elastic deformations.[28,30] Experiments on hydrogel nanoparticles have also showed that the particle rigidity affects uptake rate and pathway: soft particles enter *via* macropinocytosis, hard particles prefer the clathrin-mediated route, and in the intermediate regime both pathways are exploited, leading to a larger uptake concentration.[31]

Endocytosis also depends on particle surface chemistry and topology.[2,11,32] In particular, coarse-grained molecular dynamics simulations suggested that a long one-dimensional chain is the optimal ligand pattern for uptake when ligand densities on the particle surface are low.[33] However, the effect of ligand inhibitors that decorate the particle surface remains largely unexplored. In particular, it is unknown how inhibiting protrusions quantitatively affect particle uptake by their two-fold action of reducing the ligand density and modifying the particle morphology.

We consider a spherical and rigid particle having a fraction of ligands blocked by finite-sized inhibitors that protrude out of the spherical surface. The inhibitors represent neutralizing antibodies, peptides, or phage capsids attaching to the surface of the particle to cover (neutralize) a fraction of ligands.[25,34] When the inhibitor size vanishes, we have a spherical particle covered with active and passive ligands (*i.e.*, able and unable to bind to cell receptors, respectively). However, in general, the physical scale of the inhibitors introduces an additional geometric consideration for the successful encapsulation of the particle. We focus on the spontaneity of the wrapping process initiating endocytosis and explore the geometric determinants of the complex morphology obtained. The number and size of protrusions raise the energetic barrier for endocytosis based on particle size and inhibitor spacing due to both the reduction of ligand-receptor bindings and the additional bending penalty to wrap the inhibitors. Fig. 1 illustrates the concept of inhibiting protrusions that block the particle entry.

Building on the mechanical model for the uptake of a rigid sphere,[13] we account for the diffusivity of cell receptors across the cell membrane and the free energy of the membrane as the sum of elastic deformation energy and adhesion energy. The spontaneity of endocytosis is determined by imposing that the rate of free energy reduction, due to membrane wrapping, equals the rate of free energy dissipation due to receptor transport. We account for the reduced ligand density due to the presence of inhibitors and calculate the equilibrium configuration of the membrane wrapping around the particle and its protrusions.

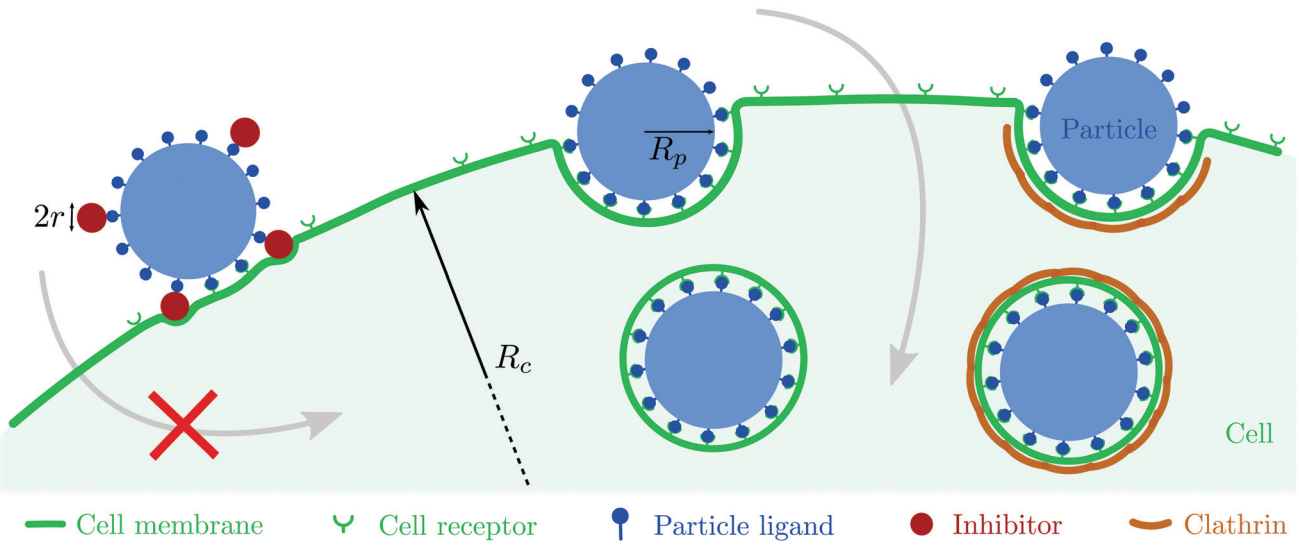

Fig. 1 Schematic illustration of the process of receptor-mediated endocytosis, including the case of clathrin coating. The presence of ligand inhibitors on the surface of a spherical particle can prevent cell entry, depending on the size and number of the inhibitors. To reduce the number of variables, we assume the cell radius R_c to be much larger than that of the particle R_p (infinite and flat cell membrane).

We find that size, indentation, and density of ligand inhibitors determine the selective uptake of particles, and the entry is completely blocked above critical thresholds. In particular, when endocytosis is independent of protein coats, particles can enter the cell only if their radius is larger than a minimum value, while for the clathrin-mediated endocytosis, particles are selected within a size range, consistently with experiments on spherical particles.[20] For the clathrin-dependent pathway, we show that the maximum radius is dictated by the clathrin coat, thus differing from the upper limit due to a shortage of cell receptors found in previous studies.[13,30]

The proposed results provide a foundation for the design of viral antibodies, peptides, and capsids acting as physical and geometrical inhibitors, and for the design of targeted nanoparticles undergoing selective cell entry based on the interplay between morphology and receptor density.

2 Methods

2.1 Particle geometry

We consider a spherical particle of radius R_p with ligands uniformly distributed on its surface with a density ξ_L. We estimate the spacing between two adjacent ligands $\sim 1/\sqrt{\xi_L}$ by assuming an ideal tessellation of the sphere consisting of a large number of hexagons and 12 pentagons (such as in Goldberg polyhedrons), see Appendix A. We denote by R the curvature radius of the membrane that wraps the spherical particle, thus including the particle radius R_p, the receptor–ligand bond, and half thickness of the lipid bilayer (1.5–2.5 nm[35]), see Fig. 2a. In the following we refer to R as the particle radius. The wrapping process requires cell receptors to diffuse towards the contact region so that the receptor density on the cell surface approximates the ligand density on the particle surface, ξ_L.

We cover a fraction p of ligands with spherical inhibitors of radius r, which we assume uniformly distributed on the particle. Such inhibitors protrude over the particle surface a length δ (see Fig. 2b), which we express as a multiple of the inhibitor radius r, *i.e.*, $\delta := 2dr$ where d is a dimensionless indentation parameter.

When the cell membrane wraps the particle, including its protrusions, the receptors diffuse toward the wrapping region to bind to the particle ligands that are still active. The surface density of effective ligands is reduced to $(1-p)\xi_L$, while the membrane will need additional area and bending to wrap around the protrusions. The surface density of receptors in the wrapped membrane is

$$\xi_p := \frac{(1-p)}{\alpha_p}\xi_L \tag{1}$$

where $\alpha_p := A_{tot}/A_s$ is the dimensionless ratio between the surface area of the membrane wrapping the whole particle with inhibiting protrusions, A_{tot}, and the surface area of the spherical particle, $A_s = 4\pi R^2$. $\alpha_p \geq 1$ measures the excess area needed for wrapping that is due to the inhibitors, with $\alpha_p = 1$ when $p = 0$ (no protrusions).

The parameter p defines the fraction of inhibited ligands and we assume that there is a maximum value $p_{max} \approx 1/\pi$, for which the wrapping process is still possible in a symmetric fashion. Indeed, above this threshold value, the number of inhibitors is so large that there must be at least two adjacent inhibitors, so that we cannot assume that the membrane wraps any protrusion by binding to the surrounding ligands, see Appendix B.

2.2 Free energy of the cell membrane and protein coat

We consider a membrane $\mathscr{S}$ with an initially uniform receptor density ξ_0, which curves to wrap a proximal particle, as cell receptors bind to particle ligands. We assume the membrane to be infinitely extended and initially flat, *i.e.* the particle radius R_p is much smaller than the cell radius R_c, namely, $R_p/R_c \ll 1$ (see Fig. 1).

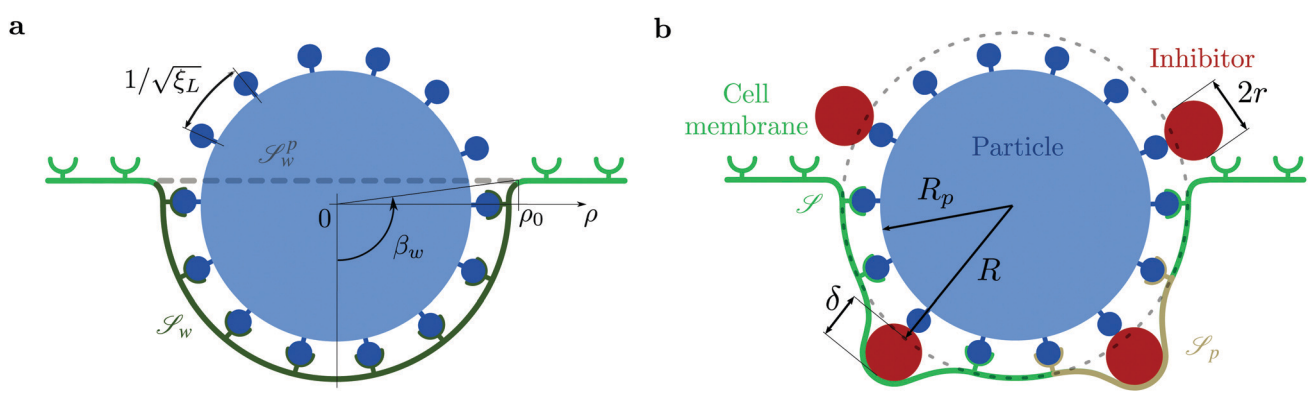

Fig. 2 Two-dimensional schematic illustration of the cell membrane $\mathscr{S}$ that wraps an external particle during receptor-mediated endocytosis. (a) Spherical particle of radius R_p with ligand surface density ξ_L, so that the spacing between two adjacent ligands is approximately $1/\sqrt{\xi_L}$, see Appendix A. The cell membrane develops a curvature of radius R, which includes both the particle and the receptor–ligand bonds. $\mathscr{S}_w$ denotes the portion of the cell membrane in contact with the particle, which corresponds to a wrapping angle β_w. $\mathscr{S}_w^p$ is the projection of $\mathscr{S}_w$ onto the flat membrane. (b) A fraction p of ligands are inhibited by spherical protrusions of radius r. Inhibitors protrude a length δ, and $\mathscr{S}_p$ denotes the representative portion of cell membrane that wraps a single protrusion, assuming protrusions are largely spaced.

Since endocytosis is often mediated by proteins – such as clathrin and caveolin – that form coated pits,[25] we include a protein coat with a spontaneous mean curvature $H^\star$, which assembles during the wrapping process and attaches to the membrane in the contact region.

The free energy of the cell membrane is given by the contributions from elastic deformation $\mathscr{E}_{\mathrm{el}}$ and adhesion $\mathscr{E}_{\mathrm{ad}}$, namely, $\mathscr{E} = \mathscr{E}_{\mathrm{el}} + \mathscr{E}_{\mathrm{ad}}$. We describe $\mathscr{E}_{\mathrm{el}}$ with the Canham–Helfrich model[36,37] and neglect deformations of the cell membrane outside the contact region $\mathscr{S}_{\mathrm{w}}$, such that

$$\mathscr{E}_{\mathrm{el}} = \int_{\mathscr{S}_{\mathrm{w}}} \left[2\kappa_{\mathrm{c}}(H - H^\star)^2 + \tilde{\kappa}_{\mathrm{c}} K\right] \mathrm{d}A + \int_{\mathscr{S}_{\mathrm{w}}} 2\kappa_{\mathrm{m}} H^2 \mathrm{d}A + \sigma \Delta A. \tag{2}$$

In eqn (2), the first integral term provides the elastic energy of the protein coat (denoted by the subscript c), whereas the other two terms provide the elastic energy of the cell membrane (denoted by the subscript m). The bending energy is expressed in terms of the mean and Gaussian curvatures, respectively H and K, with the corresponding elastic moduli κ and $\tilde{\kappa}$. The Gaussian curvature accounts for the energy stored in symmetric saddles with zero mean curvature. In view of the Gauss–Bonnet theorem, its integral over the surface reduces to the sum of a topological invariant and the integral of the geodesic curvature of the surface boundary; we neglect this term (a constant) for the infinite membrane and we consider it only for the protein coat, whose boundary evolves during wrapping. Recent experimental and theoretical evidence supports a flat-to-curved transition of the clathrin coat, with the coat assembling as a flat membrane first and then rapidly curving.[38–41] This might result from a snap-through instability,[42] interpreted as a cooperative mechanism of clathrin triskelia aiming for a constant spontaneous curvature,[43] or a time evolution of the coat bending rigidity or spontaneous curvature.[44,45] Here we assume that both the spontaneous mean curvature ($H^\star$) and the bending rigidity (κ_{c}) are constant, and we carry out a sensitivity analysis to explore their effect on the necessary condition for particle uptake. Moreover, we consider that both the membrane and the coat have the same configuration (*i.e.*, curvatures). This hypothesis implies that we neglect the coat thickness, which is about 5 nm for caveolin,[46] and 15–30 nm for clathrin.[47–49] The last term in eqn (2) describes the mechanical work due to membrane stretching, *i.e.* the product of surface tension σ to the excess area $\Delta A = A_{\mathrm{w}} - A_{\mathrm{w}}^{p}$. A_{w} is the area of the wrapping surface $\mathscr{S}_{\mathrm{w}}$, and A_{w}^{p} is the area of the corresponding projection $\mathscr{S}_{\mathrm{w}}^{\mathrm{p}}$ on the flat configuration,[50] see Fig. 2.

The adhesion energy $\mathscr{E}_{\mathrm{ad}}$ accounts for entropic, $\mathscr{E}_{\mathrm{r}}$, and enthalpic, $\mathscr{E}_{\mathrm{h}}$, contributions.[1] The configurational, entropic, energy of receptors (in analogy with an ideal gas[51]) is

$$\mathscr{E}_{\mathrm{r}} = k_{\mathrm{B}} T \int_{\mathscr{S}} \xi \ln \frac{\xi}{\xi_0} \mathrm{d}A \tag{3}$$

where k_{B} is the Boltzmann constant, T is the absolute temperature, ξ is the number of receptors per unit area of the cell membrane, and ξ_0 is the uniform receptor density in an isolated cell, or at infinite distance from the wrapping site.

The change of enthalpy, due to the formation of coated pits and the receptor–ligand binding,[13] provides the driving force for the wrapping process and is given by

$$\mathscr{E}_{\mathrm{h}} = -\int_{\mathscr{S}_{\mathrm{w}}} (\xi e_{\mathrm{RL}} + \xi_{\mathrm{c}} e_{\mathrm{c}}) \mathrm{d}A. \tag{4}$$

Here e_{RL} is the receptor–ligand binding energy, ξ_{c} is the surface density of coating protein bonds, and e_{c} is the protein binding energy.

Let us now divide each energetic contribution by $k_{\mathrm{B}}T$, and each length by the ligand spacing $\ell \approx 1/\sqrt{\xi_{\mathrm{L}}}$. The dimensionless free energy is then

$$\begin{aligned} \bar{\mathscr{E}} &= \int_{\mathscr{S}_{\mathrm{w}}} \left[2\bar{\kappa}_{\mathrm{m}} \bar{H}^2 + 2\bar{\kappa}_{\mathrm{c}} (\bar{H} - \bar{H}^\star)^2 + \bar{\tilde{\kappa}}_{\mathrm{c}} \bar{K}\right] \mathrm{d}\bar{A} + \bar{\sigma} \Delta \bar{A} \\ &\quad - \int_{\mathscr{S}_{\mathrm{w}}} (\bar{\xi} \bar{e}_{\mathrm{RL}} + \bar{\xi}_{\mathrm{c}} \bar{e}_{\mathrm{c}}) \mathrm{d}\bar{A} + \int_{\mathscr{S}} \bar{\xi} \ln(\bar{\xi}/\bar{\xi}_0) \mathrm{d}\bar{A} \end{aligned} \tag{5}$$

where $\bar{\mathscr{E}} := \mathscr{E}/(k_{\mathrm{B}}T)$, $\bar{\kappa}_i = \kappa_i/(k_{\mathrm{B}}T)$ for $i = c, m$, $\bar{H} := H/\sqrt{\xi_{\mathrm{L}}}$, $\bar{H}^\star := H^\star/\sqrt{\xi_{\mathrm{L}}}$, $\bar{\tilde{\kappa}}_{\mathrm{c}} := \tilde{\kappa}_{\mathrm{c}}/(k_{\mathrm{B}}T)$, $\bar{K} = K/\xi_{\mathrm{L}}$, $\bar{\xi} := \xi/\xi_L$, $\bar{e}_{\mathrm{RL}} := e_{\mathrm{RL}}/(k_B T)$, $\bar{\xi}_{\mathrm{c}} := \xi_{\mathrm{c}}/\xi_{\mathrm{L}}$, $\bar{e}_{\mathrm{c}} = e_{\mathrm{c}}/(k_{\mathrm{B}}T)$, $\bar{A} := \xi_{\mathrm{L}} A$, and $\bar{\sigma} := \sigma/(k_{\mathrm{B}} T \xi_{\mathrm{L}})$. In Table 1 we report the physical quantities adopted in our model, taken from literature.

In clathrin-mediated endocytosis, the self-assembling coat controls the equilibrium configuration of the bilayer – composed of membrane and coat – wrapped around the protrusion. This is due to the higher bending rigidity of the coat ($\bar{\kappa}_{\mathrm{c}} > \bar{\kappa}_{\mathrm{m}}$), as shown in Table 1. If either the coat is absent or the membrane accommodates the spontaneous curvature of

Table 1 Relevant values of the model parameters as reported in the biological literature. The thermal energy constant is $k_{\mathrm{B}}T \approx 4.14$ pN nm (at a temperature of $T = 300$ K)

Parameter	Description	Value/range	Units	Reference(s)	Used value(s)
κ_{m}	Membrane bending modulus	10–25	$k_{\mathrm{B}}T$	13, 52 and 53	$\bar{\kappa}_{\mathrm{m}} = 20$
κ_{c}	Clathrin coat bending modulus	255–315	$k_{\mathrm{B}}T$	49, 54 and 55	$\bar{\kappa}_{\mathrm{c}} = 300$
$\bar{\kappa}_{\mathrm{c}}$	Saddle-splay modulus of clathrin coat	n.a.	$k_{\mathrm{B}}T$	n.a.	$\bar{\kappa}_{\mathrm{c}} = 0$
ξ_0	Cell receptor density	5×10^{-5}–130×10^{-5}	nm^{-2}	13 and 30	$\bar{\xi}_0 = 0.025, 0.1$
ξ_{L}	Particle ligand density	3×10^{-3}–20×10^{-3}	nm^{-2}	13 and 30	$\bar{\xi}_{\mathrm{L}} = 5 \times 10^{-3}$
e_{RL}	Receptor–ligand binding energy	10–25	$k_{\mathrm{B}}T$	30	$\bar{e}_{\mathrm{RL}} = 15$
e_{c}	Binding energy per clathrin triskelion	5–30	$k_{\mathrm{B}}T$	49, 53 and 56	$\bar{e}_{\mathrm{c}} = 23$
ξ_{c}	Density of clathrin triskelia	1.25×10^{-3}	nm^{-2}	49	$\bar{\xi}_{\mathrm{c}} = 0.25$
σ	Membrane tension	5×10^{-3}	$k_{\mathrm{B}}T\ \mathrm{nm}^{-2}$	50	$\bar{\sigma} = 1$
$R^\star$	Preferred radius of clathrin-coated pit	32.5–90	nm	43, 49, 57 and 58	$\bar{H}^\star = -0.283$

the coat, then the elastic term is dominated by the cost of bending the cell membrane, since its rigidity, $\bar{\kappa}_m$, is one order of magnitude larger than its tension, $\bar{\sigma}$, see Table 1. The adhesion energy is of the same order of magnitude of the elastic energy, with the enthalpic term dominating over the entropic one. Indeed, in the wrapping region, $\bar{\xi} \approx 1$ is one order of magnitude smaller than the binding energies $\bar{e}_{RL}$ and $\bar{e}_c$. From this analysis we observe that the process is primarily led by an exchange of enthalpic (binding) energy, $\bar{\mathscr{E}}_h$, with elastic (wrapping) energy, $\bar{\mathscr{E}}_{el}$.

In comparison with a spherical particle, the presence of protrusions hinders the process of endocytosis by increasing the energetic cost of wrapping. Each protrusion raises $\mathscr{E}_{el}$ by increasing membrane curvature locally. Protrusions also affect the adhesion energy $\mathscr{E}_{ad}$ by reducing the enthalpic gain and the entropic cost, due to the loss of a fraction p of receptors in the wrapped region. This can be seen from $\xi_p < \xi_L$ in eqn (1) and the last two terms of eqn (5). The reduced cost favors endocytosis, but is lower than the reduced gain, which finally provides an additional barrier to particle uptake. In the following section we provide quantitative evidence of this scaling argument.

2.3 Condition for endocytosis

Spherical particle. We assume that cell receptors are mobile and diffuse towards the contact site to bind to (immobile) particle ligands. We assume that receptors are uniformly distributed with a surface density ξ_0 at remote distances from the binding site. They accumulate in the contact region to match the surface density of ligands, $\xi_L > \xi_0$. This yields a depletion of receptors in the outer proximity of the contact front, which determines a concentration gradient that drives the global diffusion towards the binding site.[13,51]

We describe the nonuniform receptor density outside the contact region with the function $\xi(\rho, t)$, where ρ is the radial coordinate and t is time. We denote by $\rho_0(t)$ the radial coordinate of the moving contact front, which is given by $\rho_0(t) = R\sin\beta_w(t)$, where $\beta_w(t)$ is the angle that corresponds to the surface area $A_w(t)$ of the portion of the cell membrane that wraps the particle, $\mathscr{S}_w(t)$ (see Fig. 2a).

During the wrapping process, receptors are driven by a local reduction in the free energy, which rate of change is

$$\begin{aligned}\mathscr{E}(t) &= -2\pi D k_B T \int_{\rho_0(t)}^{+\infty} \xi \left(\frac{\partial \ln \xi}{\partial \rho}\right)^2 \rho \, d\rho \\ &- \dot{A}_w(t)\Bigg\{\xi_L e_{RL} + \xi_c e_c - k_B T \xi_L \left(\ln\frac{\xi_L}{\xi_0} + \ln\frac{\xi_0}{\xi_+} - 1 + \cos\beta_w \frac{\xi_+}{\xi_L}\right) \\ &- \frac{1}{R^2}\left[2\kappa_m + 2\kappa_c(1 - R/R^\star)^2 + \tilde{\kappa}_c\right] - k_B T(1 - \cos\beta_w)\sigma\Bigg\}\end{aligned} \tag{6}$$

as explained in Appendix C with $p = 0$. Here a superposed dot denotes time differentiation, D is the diffusivity of cell receptors, $R^\star$ is the preferred radius of curvature of the protein coat, and $\xi_+ := \lim_{\rho\to\rho_0^+} \xi(\rho)$ is the receptor density in the unwrapped region next to the binding site ρ_0^+, giving $\xi_+ < \xi_0$.[51]

The integral term in eqn (6) is the rate of energy dissipation due to receptor transport.[51] The expression within $\{\ldots\}$ describes the rate of free energy change per unit of new wrapping membrane. The first two terms represent the reduction of enthalpy (receptor–ligand bindings and coat assembling). The expression within $(\ldots)$, and multiplied by ξ_L, accounts for the entropic change: the first two terms describe the relocation of receptors from the uniform density ξ_0 to ξ_L, within the wrapped region, and ξ_+, outside that region; the other two terms describe the receptor transport across the front, from ξ_+ to ξ_L, where ξ_+ is multiplied by $\cos\beta_w$ to account for the difference between the spherical area and its planar projection. The terms within $[\ldots]$ define the free energy increment required to deform elastically the membrane and the protein coat. Finally, the term multiplied by σ accounts for the membrane tension, which increases with the wrapping angle β_w.

Particle wrapping can occur only if the free energy is released at a rate greater than the rate of energy dissipated by the cell receptor transport across the membrane.[51] From this, we determine the necessary condition for initiating particle wrapping *via* eqn (6), by approximating the density ξ_+ with the initial density ξ_0, and by setting $\beta_w = 0$, giving

$$\begin{aligned}&\left(\bar{e}_{RL} + \bar{\xi}_c \bar{e}_c + 1 - \bar{\xi}_0 + \ln\bar{\xi}_0\right)\bar{R}^2 > 2\bar{\kappa}_m \\ &\quad + 2\bar{\kappa}_c(1 - \bar{R}/\bar{R}^\star)^2 + \bar{\tilde{\kappa}}_c\end{aligned} \tag{7}$$

with $\bar{R}^\star := R^\star\sqrt{\xi_L}$. If we neglect the protein coat, eqn (7) reduces to the condition found by Gao *et al.*[13] In this case, if the expression within the parenthesis on the left side is positive – *i.e.*, the enthalpic gain is higher than the entropic cost – the inequality is satisfied for any value of the dimensionless radius larger than a threshold, $\bar{R} > \bar{R}_{min}$. By fixing the value of the ligand density, this translates to the existence of a minimum radius R_{min} for the particle uptake. For protein-independent receptor-mediated endocytosis and for relevant biological values of the parameters (see Table 1), the minimum radius is $R_{min} \approx 24$ nm, which is in agreement with experimental observations.[13]

In the presence of a protein coat, the same holds true for values of the preferred radius of curvature that are higher than a threshold $\left(\bar{R}^\star > \bar{R}_0^\star\right)$, such that for particles that are large enough, the driving force is sufficient to overcome the penalty for deviating from $\bar{R}^\star$. However, for higher values of the spontaneous curvature of the protein coat $\left(\bar{R}^\star < \bar{R}_0^\star\right)$, the cost of deviating from the preferred configuration is increasing faster than the driving force, for particles of increasing radii. This implies also an upper bound on the dimensionless radius, $\bar{R}_{max}$. Shifting perspective, for any fixed spontaneous curvature, there exists a critical value of the coat's bending rigidity $\bar{\kappa}_{c,0}$, above which the uptake is restricted to particles between a minimum and a maximum radii. In other terms, if the protein coat has a preferred radius smaller than $\bar{R}_0^\star$ (or a bending rigidity higher than $\bar{\kappa}_{c,0}$), the cost of bending dominates over adhesion and becomes prohibitive for radii larger than a maximum value. In this case, the wrapping is favorable only

for particles within a specific size range, $\bar{R} \in (\bar{R}_{\min}, \bar{R}_{\max})$, see Appendix D.

For relevant values of the biological parameters for clathrin-mediated endocytosis (see Table 1), the critical preferred radius is $R_0^\star \approx 78.76$ nm $(R_0^\star \approx 81.57$ nm$)$ for $\bar{\kappa}_c = 300$ and $\bar{\xi}_0 = 0.1$ ($\bar{\xi}_0 = 0.025$), *cf.* Appendix D. Thus, by assuming a preferred radius of curvature $R^\star = 50$ nm, we predict the uptake of particles of radius between $R_{\min} \approx 33$ nm ($R_{\min} \approx 34$ nm) and $R_{\max} \approx 134$ nm ($R_{\max} \approx 126$ nm) for $\bar{\xi}_0 = 0.1$ ($\bar{\xi}_0 = 0.025$). This theoretical conclusion is in good agreement with experimental observations about the size dependence of clathrin-mediated endocytosis that exhibited an upper radius limit for internalization of approximately 100 nm.[20] In addition, the maximum radius found differs from the one previously proposed as the result of a limitation in the number of available receptors, which is $R_{\max}^{(0)} := L\sqrt{\bar{\xi}_0}/2$ where L denotes the radius of the finite membrane available;[13,30] in this case, for a typical radius of $L = 10$ μm, we get a maximum radius $R_{\max}^{(0)} \approx 1580$ nm ($R_{\max}^{(0)} \approx 790$ nm) for $\bar{\xi}_0 = 0.1$ ($\bar{\xi}_0 = 0.025$), which is much larger than the maximum radius due to the clathrin coat.

Spherical particle with protruding inhibitors. We adapt the argument sketched above for the spherical particle, by splitting the cell membrane into regions that wrap a single protrusion and the rest that adheres to the spherical part of the particle, see Fig. 2b. As shown in Appendix C, we arrive at the inequality

$$\begin{aligned}
&(1-p)\xi_L e_{RL} + \alpha_p \xi_c e_c \\
&\quad + k_B T \xi_L \left[(1-p) - \frac{\xi_0}{\xi_L} + (1-p)\ln\left(\frac{\alpha_p}{1-p}\frac{\xi_0}{\xi_L}\right)\right] \\
&\quad > k_B T(\alpha_p - 1)\sigma + \left(1 - \frac{p}{p_{\max}}\right)\left[2\kappa_m + 2\kappa_c\left(1 - \frac{R}{R^\star}\right)^2 + \tilde{\kappa}_c\right]\frac{1}{R^2} \\
&\quad + p\xi_L \int_{\mathscr{S}_p} \left[2\kappa_m H^2 + 2\kappa_c (H - H^\star)^2 + \tilde{\kappa}_c K\right] \mathrm{d}A,
\end{aligned} \tag{8}$$

where $1/p_{\max} = 2\pi\bar{R}^2\,(1 - \cos 1/\bar{R})$, see Appendix B. Eqn (8) provides a necessary condition for the initiation of wrapping for a particle with inhibiting protrusions, and reduces to eqn (7) for $p = 0$.

To solve eqn (8) we need to obtain the equilibrium configuration of the membrane in the region that wraps a protruding inhibitor, $\mathscr{S}_p$. This reduces to the solution of an obstacle problem that implicitly depends on the geometry of the particle, namely, r (protrusion radius), R, and δ (indentation), see Fig. 2b. The equilibrium configuration is the one that minimizes the elastic deformation energy, $\mathscr{E}_{el}$, while satisfying compatibility with the protrusion and adhering to the particle at the boundary, due to the surrounding receptor–ligand bonds. This requires the solution of a nonlinear variational inequality, which we approximate numerically, since analytical results are unavailable. In this study we used the finite element method[59] to minimize the elastic energy with a penalty term that enforces the obstacle constraint,[60] described as a half spherocylinder in the Monge parametrization, see Appendix F and Fig. 3.

In this analysis, we assumed that the membrane wraps the protrusions and binds to the closest effective ligands. This hypothesis is realistic for small p and small r, where a single-spaced configuration is energetically favorable. In fact, for larger r, a double-spaced configuration is favored over the single-spaced one (see Appendix F).

3 Results

By solving for the equality in eqn (8) in the parameter space $(p, \bar{R})$ we determine the regions where endocytosis is favorable, using the parameters reported in Table 1. Fig. 4a shows the results in the absence of clathrin coat, whereas, Fig. 5a shows the results in the presence of the coat.

In the absence of inhibitors ($p = 0$), the wrapping process starts only if the particle radius lies within the specific range $R_{\min} < R < R_{\max}$, with $R_{\max} \to \infty$ in the absence of protein coat. In the case of inhibitors ($p > 0$) without protrusions ($\bar{r} = 0$), the range size $(R_{\min}, R_{\max})$ slightly contracts for moderate values of p (see Fig. 4a and 5a). Finally, the presence of

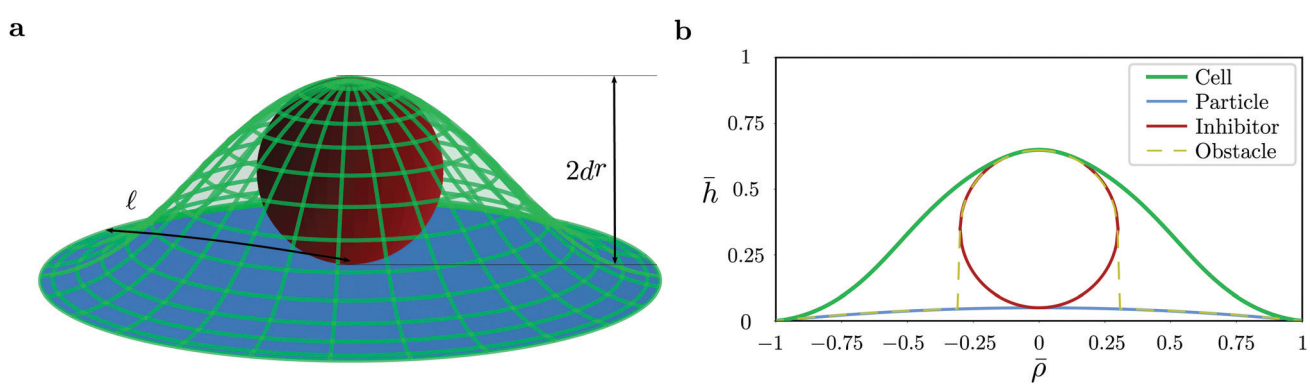

Fig. 3 (a) Three-dimensional and (b) two-dimensional views of cell membrane clamped to the particle at the boundary and wrapping the ligand inhibitor. Both the radial coordinate, $\bar{\rho}$ and the height function $\bar{h}$ are measured in units of the ligand spacing $\ell \approx 1/\sqrt{\xi_L}$. We determined the configuration as an axisymmetric solution to the obstacle problem where the obstacle is defined as half capsule (yellow dashed line), for model parameters $\ell \approx 14$ nm, $\bar{r} := r\sqrt{\xi_L} = 0.3$, $\bar{R} = 10$, $d = 1$, $\bar{\kappa}_m = 20$, $\bar{\kappa}_c = \bar{\tilde{\kappa}}_c = \bar{H}^\star = 0$, see Appendix E.

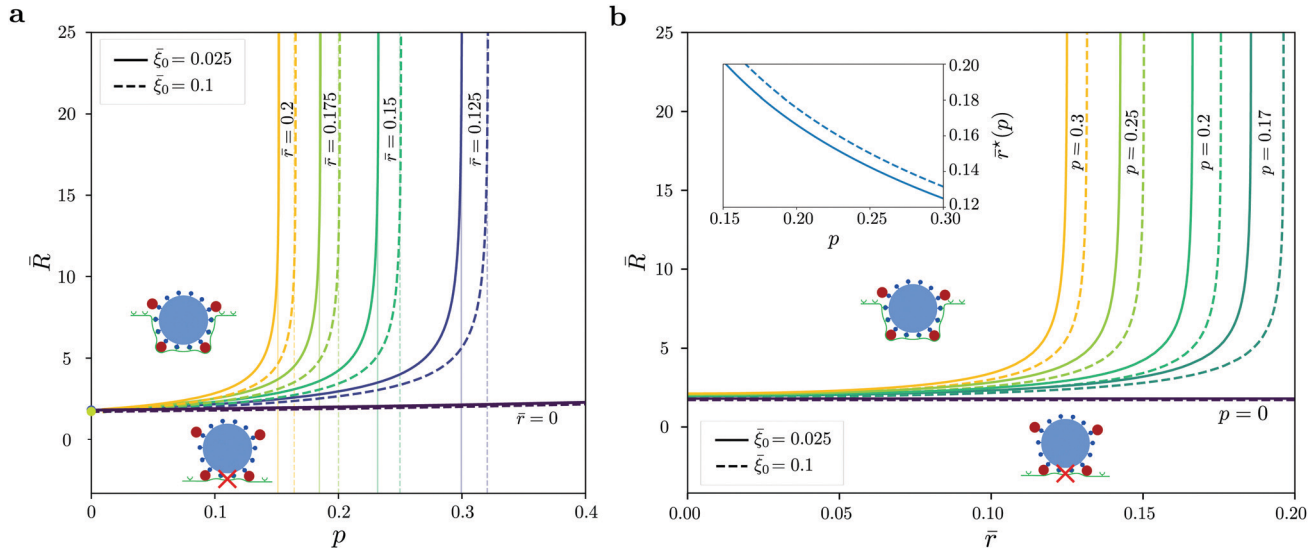

Fig. 4 Regions of (un)favorable endocytosis determined from eqn (8) in the case of the receptor-mediated pathway without protein coat for model parameters $d = 1$, $\bar{e}_{RL} = 15$, $\bar{\sigma} = 1$, $\xi_L = 5 \times 10^{-3}$ nm^{-2}, and $\bar{\kappa}_c = \bar{\bar{\kappa}}_c = \bar{e}_c = \bar{H}^\star = 0$. (a) Parameter space ($p$, $\bar{R}$) where p is the fraction of inhibited ligands and $\bar{R} := R\sqrt{\xi_L}$ is the dimensionless particle radius. Region boundaries are for different dimensionless obstacle sizes, $\bar{r} := r\sqrt{\xi_L}$, and ratios between ligand and receptor densities, $\bar{\xi}_0 := \xi_0/\xi_L$. The curve provides the minimum radius $\bar{R}_{min}$ and endocytosis is favored when $\bar{R} > \bar{R}_{min}$. Vertical lines show the critical values of p that correspond to the limit case of $\bar{R}_{min} \to \infty$. Dots on the axis $p = 0$ indicate the minimum radii previously found.[13] (b) Parameter space ($\bar{r}$, $\bar{R}$) where $\bar{r}$ is the dimensionless obstacle sizes, $\bar{r} = r\sqrt{\xi_L}$ and $\bar{R} := R\sqrt{\xi_L}$ is the dimensionless particle radius. Region boundaries are for different fractions of inhibited ligands p, and ratios between ligand and receptor densities, $\bar{\xi}_0 := \xi_0/\xi_L$. The inset shows the critical inhibitor size $r^\star(p)$ above which endocytosis is completely blocked, as function of p.

protruding inhibitors ($p > 0$ and $\bar{r} > 0$) significantly shrinks the range of admissible radii until their density p reaches a critical value $p^\star = p^\star(\bar{r})$, above which the particle uptake is completely blocked. This shows the crucial impact of the inhibitor size $\bar{r}$ for moderate values of the fraction of inhibited ligands p. As observed in Fig. 4a and 5a, $p^\star$ is inversely related to $\bar{r}$. For the coat-independent case, we can calculate such a threshold by solving the equality at eqn (8) for $\bar{R} \to \infty$ and different values of $\bar{r}$ (see Fig. 4a). In particular, we can write $p^\star$ explicitly for $\bar{r} = 0$ (see Appendix G) and, with the parameters reported in Table 1, we find $p^\star(\bar{r} = 0) \approx 0.995$ for $\bar{\xi}_0 = 0.1$, and $p^\star(\bar{r} = 0) \approx 0.999$ for $\bar{\xi}_0 = 0.025$.

Analogously, for a given inhibitor density p the inhibitor size $\bar{r}$ controls the range of particles for which the wrapping can initiate, and above a critical size $\bar{r}^\star = \bar{r}^\star(p)$ the process is completely blocked. Fig. 5 shows that for small protrusion sizes $\bar{r}$, the selected size range is almost independent of moderate densities p, while this becomes relevant for larger protrusions.

In both Fig. 4b and 5b, the range of radii (R_{min}, R_{max}) is asymmetric with respect to the preferred radius of curvature of the coat $R^\star$. This is due to the cost of bending the cell membrane, which diverges for $\bar{R} \to 0$ but vanishes for $\bar{R} \to +\infty$, thus determining a lower bound but not an upper bound. It is the protein coat that introduces an upper bound in the particle size, because of its spontaneous curvature. To further explore the impact of the coat on the conditions for the particle uptake, we vary $\bar{\kappa}_c$, the bending rigidity (Fig. 6a), and $\bar{R}^\star$, the radius of the preferred curvature (Fig. 6b). Qualitatively, the phase diagrams of endocytosis transition from the ones of the clathrin-independent pathway in Fig. 4a to the ones of the clathrin-mediated pathway in Fig. 5a, as either the bending rigidity or the spontaneous curvature increases. In particular, for the case of spherical particles ($p = 0$), the maximum radius for the uptake emerges beyond the predicted critical values of the coat bending rigidity ($\bar{\kappa}_{c,0}$) in Fig. 6a, and the coat preferred curvature ($1/\bar{R}_0^\star$) in Fig. 6b, *cf.* Appendix D.

Finally, similar results follow by varying the indentation parameter d of the spherical inhibitors, while keeping fixed their size $\bar{r}$. This corresponds to spherical inhibitors that protrude only partially, for $d < 1$, or that are raised above the particle surface, for $d > 1$ (see Fig. 3). For any fixed inhibitor size, the uptake is blocked more effectively when inhibitors protrude to a greater degree out of the particle surface, see Fig. 7. We explain this result as a consequence of an increase in the elastic cost, which is needed to wrap more pronounced protrusions. Indeed, the indentation parameter d ultimately affects the geometry of the obstacle, which determines the configuration of the membrane and hence the integral term appearing in eqn (8). Thus, different geometries are equivalent in terms of the necessary condition for the wrapping given by eqn (8). Fig. 7 shows contour plots of $\bar{R}_{min}$ in the space of parameters that define the geometry of the protruding inhibitor, (d, $\bar{r}$), for the case of coat-independent endocytosis and for a fixed inhibitor density. As expected, the minimum radius is maximum when both the indentation and the size of the inhibitor are maximum, since such a configuration raises the cost of bending the cell membrane. Moreover, an increase in the fraction of inhibited ligands, p, has the effect of

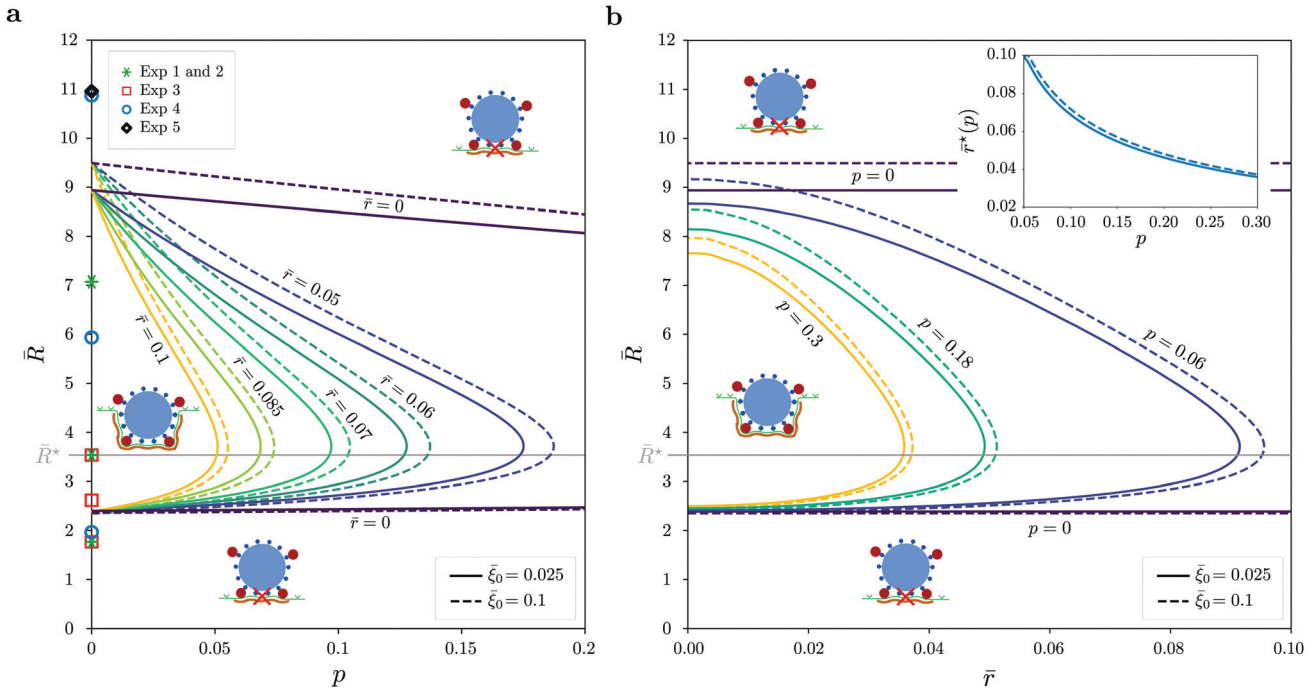

Fig. 5 Regions of (un)favorable endocytosis determined from eqn (8) in the case of clathrin-dependent pathway for model parameters d = 1, $\bar{e}_{RL}$ = 15, $\bar{\sigma}$ = 1, $\xi_L = 5 \times 10^{-3}$ nm^{-2}, $\bar{H}^\star \approx -0.283$, $\bar{\kappa}_c = 300$, $\bar{\bar{\kappa}}_c = 0$, and $\bar{e}_c$ = 23. (a) Parameter space (p, $\bar{R}$) where p is the fraction of inhibited ligands and $\bar{R} := R\sqrt{\xi_L}$ is the dimensionless particle radius. Region boundaries are for different dimensionless obstacle sizes, $\bar{r} := r\sqrt{\xi_L}$, and ratios between ligand and receptor densities, $\bar{\xi}_0 := \xi_0/\xi_L$. The curve defines the minimum and maximum radii, $\bar{R}_{min}$ and $\bar{R}_{max}$, and endocytosis is favored when $\bar{R}_{min} < \bar{R} < \bar{R}_{max}$. The horizontal (grey) line reports the dimensionless radius of spontaneous curvature of the clathrin coat $\bar{R}^\star = 1/|\bar{H}^\star| \approx 3.53$. Dots on the axis p = 0 correspond to radii of spherical nanoparticles internalized *via* clathrin-mediated endocytosis as reported in literature: Exp 1,[20] Exp 2,[22] Exp 3,[21] Exp 4,[23] and Exp 5.[61] (b) Parameter space ($\bar{r}$, $\bar{R}$) where $\bar{r}$ is the dimensionless obstacle sizes, $\bar{r} := r\sqrt{\xi_L}$ and $\bar{R} := R\sqrt{\xi_L}$ is the dimensionless particle radius. Region boundaries are for different fractions of inhibited ligands p, and ratios between ligand and receptor densities, $\bar{\xi}_0 := \xi_0/\xi_L$. The inset shows the critical inhibitor size $r^\star(p)$ above which endocytosis is completely blocked, as function of p.

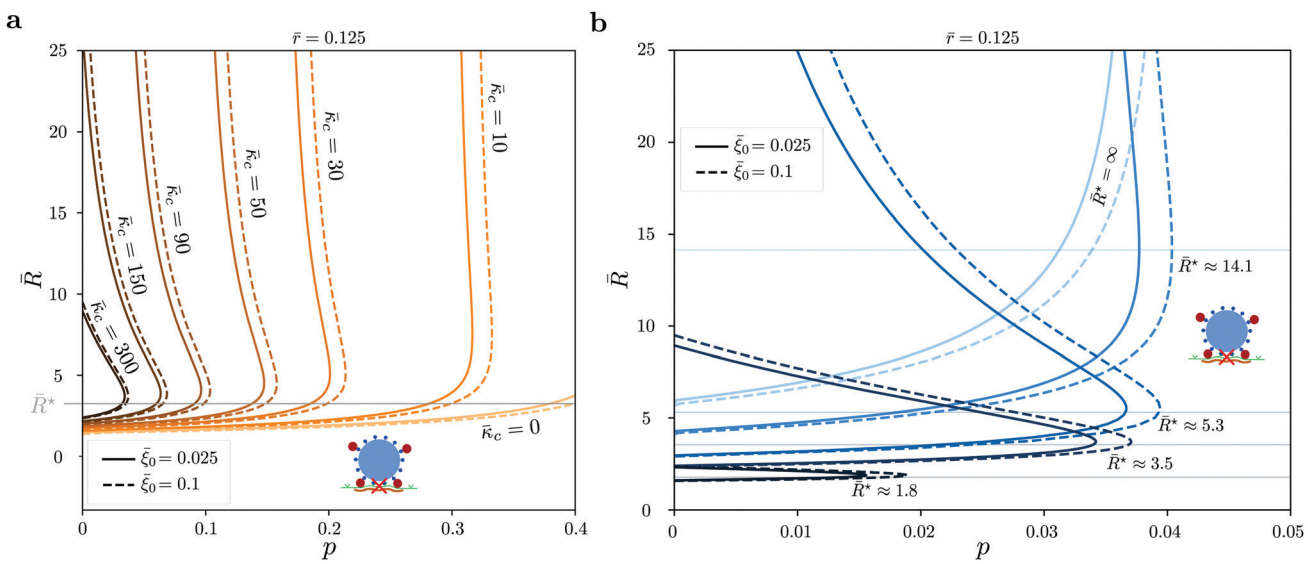

Fig. 6 Regions of (un)favorable endocytosis in the parameter space (p, $\bar{R}$) where p is the fraction of inhibited ligands and $\bar{R} := R\sqrt{\xi_L}$ is the dimensionless particle radius. Region boundaries are determined from eqn (8) for the clathrin-dependent pathway with model parameters $\bar{r}$:= 0.125, d = 1, $\bar{e}_{RL}$ = 15, $\bar{\sigma}$ = 1, $\xi_L = 5 \times 10^{-3}$ nm^{-2}, $\bar{\kappa}_c$ = 0, $\bar{e}_c$ = 23, and for two values of the ratio between ligand and receptor densities, $\bar{\xi}_0 := \xi_0/\xi_L$. (a) The coat has constant mean spontaneous curvature $\bar{H}^\star \approx -0.283$, whereas its rigidity κ_c spans the range from $0k_BT$ to $300k_BT$. (b) The coat has constant rigidity $\bar{\kappa}_c = 300$, whereas its spontaneous radius of curvature $\bar{R}^\star$ spans the range from 1.8 to $+\infty$.

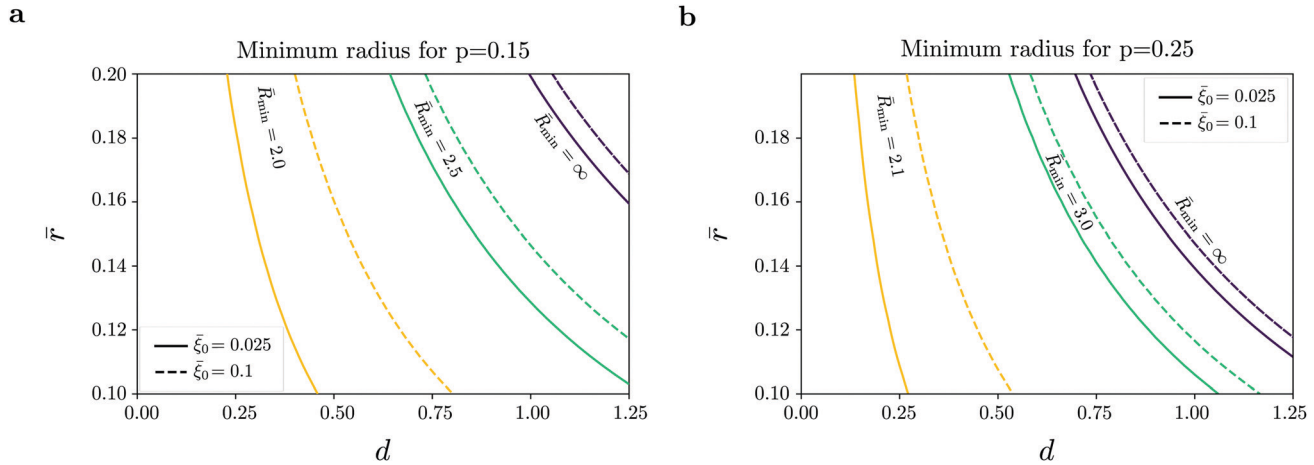

Fig. 7 Level curves of the dimensionless minimum particle radius $(\bar{R}_{\min} = R_{\min}\sqrt{\bar{\xi}_L})$ for favorable endocytosis as a function of the dimensionless radius of the inhibitor, $\bar{r} := r\sqrt{\bar{\xi}_L}$, and d. The indentation depth of the protrusion in the membrane, from the surface of the particle, is $\delta = 2dr$ (see Fig. 2). Endocytosis is completely blocked by protrusions with parameters in the region on the right of the curves for $\bar{R}_{\min} = \infty$. The results are for different values of the receptor density $\bar{\xi}_0$ and the fraction of inhibited ligands p. Model parameters are $\bar{e}_{RL} = 15$, $\bar{\sigma} = 1$, $\xi_L = 5 \times 10^{-3}$ nm^{-2}, $\bar{\kappa}_c = \bar{\tilde{\kappa}} = \bar{e}_c = 0$ (no protein coat), and (a) $p = 0.15$ (b) $p = 0.25$.

further blocking the process of endocytosis, so that higher values of p correspond to higher values of the minimum radius, see Fig. 7.

4 Discussion and conclusions

We found that the cost of bending the cell membrane and the protein coat, if present, is a determining factor for the inhibition of particle wrapping during the process of endocytosis. For the case of clathrin-mediated endocytosis, the cost of bending the cell membrane implies the existence of a minimum radius, while a maximum radius arises from the cost of bending the clathrin coat, due to its preferred curvature and bending rigidity.

In the presence of ligand inhibitors, the wrapping process depends on the radius and indentation depth of their protrusion, as well as their density. This reduces the size range of particles for which the wrapping process can initiate. Moreover, for a given inhibitor density, the uptake is completely blocked when the radius and indentation depth of the inhibitor are above given thresholds (see Fig. 7).

We analyzed the case of a spherical particle with uniformly distributed protruding inhibitors. Real biological systems are expected to exhibit random distribution of inhibitors/protrusions, hence our model provides a coarse-grained analysis over a large population of particles/viruses. The current study provides a simple way to estimate the efficacy of ligand inhibitors in selectively blocking endocytosis in the presence and in the absence of protein (clathrin) coats. A possible avenue for future research regards the optimal distribution of ligand inhibitors to block the particle uptake. As the inhibitor size vanishes, this question reduces to the case of a spherical particle with a fraction of active ligands, for which a one-dimensional chain would be the most efficient pattern for the uptake.[33]

When specialized to the case of spherical particles without protrusions, our results agree with experimental observations on clathrin-mediated endocytosis,[20–23] and are consistent with theoretical findings in the absence of clathrin,[13] see Fig. 4 and 5. However, a complete quantitative validation of our findings is difficult, due to the lack of experiments on the morphology considered in this study, namely, spherical particles with protrusions unable to bind to the cell membrane. A possible validation could be carried out by testing the uptake of single nanoparticles with different morphological parameters, such as nanoparticle size and inhibitor density, size, or shape.

We derived a necessary condition for the uptake of a particle by requiring that the free energy reduction rate is higher than the dissipation rate due to the diffusion of receptors, thus neglecting other forms of dissipation that would provide additional energetic barriers. In particular, we assumed that deformations during the wrapping process are much slower than the relaxation dynamics of the membrane, and hence the model does not account for any dissipation due to the viscous nature of lipid membranes.[62] In addition, a more detailed model could explicitly include the entropic cost of clathrin recruitment (proportional to the mismatch in clathrin protein density between the wrapping site and the cytoplasm) and hence the dissipation due to the clathrin transport. However, this would result in an additional cost due to the relocation of clathrin triskelia, which can be accounted for by simply reducing the net binding energy e_c of clathrin in the present model.

A further barrier to the wrapping might result from elastic deformations outside the contact region, which, in fact, we expect to be negligible at the initiation of the process, and only marginally relevant for rigid particles,[30,63] since the membrane would likely assume catenoid-like configurations of nearly zero bending energy.[64] We also neglected the effect of actin and BAR proteins, considered elsewhere in the context of clathrin-mediated endocytosis.[42,65] However, it should be noted that,

while some studies have investigated the role of actin in this process,[66] clathrin appears the main driver in mammalian cell endocytosis.[67,68] This excludes the case when high surface tension in the cell membrane may overcome the driving force provided by clathrin unless actin intervenes to initiate endocytosis, as observed in yeast cells.[69] A clear picture of the role of BAR proteins in the initiation and scission of the delivery vesicle in clathrin-mediated endocytosis has yet to emerge.[68] The theoretical approach developed here could be adapted to model the abovementioned mechanisms, other entry pathways, such as the one involving caveolin, and also removal processes (exocytosis),[70] but these questions are beyond the scope of the present study.

In conclusion, it is worth emphasizing the potential implications of the present study. Our model provides a tool for the design of novel molecular strategies for the morphological control of endocytosis, with applications ranging from viral antibodies to engineered nanoparticles for targeted diagnostics and therapeutics. In the context of the design of viral antibodies, our results provide an estimate of the minimum density of ligands to be inhibited to prevent the virus from entering the cell. Instead, in the context of nanomedicine, protrusions might represent a morphological feature of the delivering nanoparticle, designed to enter only targeted cells.

Author contributions

M. B. designed the research; D. A. performed the research; D. A., G. J. E., and M. B. wrote the paper.

Conflicts of interest

There are no conflicts to declare.

Appendices

A Spacing between particle ligands

For a large number $N \approx 4\pi R^2 \xi_L$ of ligands, we approximate the sphere of radius R with a polyhedron with $H \approx N/3$ hexagons of area $A_H = 3\sqrt{3}\ell^2/2$. By comparing the surface areas of the polyhedron and the sphere, namely,

$$4\pi R^2 \approx 2\sqrt{3}\pi R^2 \ell^2 \xi_L, \tag{A.1}$$

we arrive at $\ell \sim \xi_L^{-1/2}$, which we adopt in our model as the spacing between two ligands.

B The maximum number of inhibitors

In this study we assume that the wrapping process of the particle with inhibitors is driven by receptor–ligand binding around the protrusion. This condition is possible for the fraction of inhibited ligands p that is below a critical value $p_{\max}$, to assure the presence of a sufficient number of active ligands. Each protrusion is associated with a surface area of $\sim 2\pi R^2 (1 - \cos \ell/R)$ on the sphere. In the limit case of $p = p_{\max}$, there are at most

$$N_i \approx \frac{4\pi R^2}{2\pi R^2(1-\cos \ell/R)} = \frac{2}{(1-\cos \ell/R)} \tag{B.1}$$

inhibitors for $N \approx 4\pi R^2 \xi_L$ ligands. Because $p = N_i/N$, from eqn (B.1), we define

$$p_{\max} := \frac{1}{2\pi \bar{R}^2(1-\cos 1/\bar{R})}. \tag{B.2}$$

In the limit of a large dimensionless radius $\bar{R} := R\sqrt{\xi_L}$, we get $p_{\max} \approx 1/\pi$. We observe that this is approximately in agreement with the hexagonal distribution, for which each ligand is adjacent to 3 protrusions, such that each protrusion is associated with 2 ligands and $p_{\max} \approx 1/3$.

C Condition for endocytosis

In this section we derive the condition for endocytosis of a particle with protruding inhibitors. The free energy of the cell membrane is the sum of the surface free energy density integrated over the contact region $\mathscr{S}_w$, and over the remaining area of the membrane, $\mathscr{S}\backslash\mathscr{S}_w$, giving

$$\begin{aligned}\bar{\mathscr{E}} = &\int_{\mathscr{S}_w} \Big\{ \Big[2\bar{\kappa}_m \bar{H}^2 + 2\bar{\kappa}_c(\bar{H}-\bar{H}^\star)^2 + \bar{\bar{\kappa}}_c \bar{K}\Big] - \big(\bar{\xi}_p \bar{e}_{RL} + \bar{\xi}_c \bar{e}_c\big) \\ &+ \bar{\xi}_p \ln\big(\bar{\xi}_p/\bar{\xi}_0\big)\Big\} \mathrm{d}\bar{A} + \int_{\mathscr{S}\backslash\mathscr{S}_w} \bar{\xi} \ln\big(\bar{\xi}/\bar{\xi}_0\big)\mathrm{d}\bar{A} + \bar{\sigma}\Delta\bar{A}\end{aligned} \tag{C.1}$$

with the notation introduced in the main text. In particular, we recall that ξ_p is the receptor density on the cell membrane in the contact region given by eqn (1).

Splitting the wrapping region $\mathscr{S}_w$ into representative regions, $\mathscr{S}_p$, wrapping one single protrusion, and the remaining surface adhering to the spherical part of the particle, from eqn (1) and (C.1) we have

$$\begin{aligned}\bar{\mathscr{E}} = &-\bar{A}_w\left[\frac{1-p}{\alpha_p}\left(\bar{e}_{RL} + \ln\frac{\alpha_p \bar{\xi}_0}{1-p}\right) + \bar{\xi}_c \bar{e}_c\right] \\ &+ \frac{p\bar{A}_w}{\alpha_p}\int_{\mathscr{S}_p}\Big[2\bar{\kappa}_m \bar{H}^2 + 2\bar{\kappa}_c(\bar{H}-\bar{H}^\star)^2 + \bar{\bar{\kappa}}_c \bar{K}\Big]\mathrm{d}\bar{A} \\ &+ \left(1 - \frac{p\bar{A}_p}{\alpha_p}\right)\frac{\bar{A}_w}{\bar{R}^2}\Big[2\bar{\kappa}_m + 2\bar{\kappa}_c(1-\bar{R}/\bar{R}^\star)^2 + \bar{\bar{\kappa}}_c\Big] \\ &+ \bar{\sigma}\Delta\bar{A} + 2\pi\int_{\bar{\rho}_0(t)}^{\infty} \bar{\xi}\ln\big(\bar{\xi}/\bar{\xi}_0\big)\bar{\rho}\,\mathrm{d}\bar{\rho}.\end{aligned} \tag{C.2}$$

Here we used the polar coordinate ρ (given the axial symmetry of the problem) to rewrite the integral over the unwrapped (flat) region $\mathscr{S}\backslash\mathscr{S}_w$ with ρ_0 the radius of the projection of $\mathscr{S}_w$ on the plane, $\mathscr{P}_w^p$ (see Fig. 2a).

During wrapping the contact area A_w increases with time and ρ_0 varies accordingly. For protrusions of small size, r, with respect to the particle radius, R, we have

$$\rho_0 \approx R\sin\beta_w \tag{C.3}$$

where β_w is the contact (wrapping) angle (Fig. 2a). Moreover,

$$\bar{A}_w\left(1-\frac{p}{\alpha_p}\Delta\bar{A}_p\right) = 2\pi\bar{R}^2(1-\cos\beta_w) \tag{C.4}$$

where $\Delta\bar{A}_p := A_p - A_p^s$ is the difference between the surface area of $\mathscr{S}_p$ (A_p) and the one of its projection on the spherical particle (A_p^s). Combining eqn (C.3) and (C.4), we arrive at

$$\bar{\rho}_0{}^2 = \frac{\bar{A}_w}{\pi\alpha_p}\left(1-\frac{\bar{A}_w}{4\pi\bar{R}^2\alpha_p}\right). \tag{C.5}$$

Following *Freund and Lin,*[51] we assume that receptors diffuse through the cell membrane according to the second Ficks law giving the rate of change of receptor density as $\dot{\xi} = D\Delta\xi$, where D is the diffusion coefficient and a dot denotes the time derivative. In axial symmetry this equation reads as

$$\dot{\xi} = \frac{D}{\rho}\frac{\partial}{\partial\rho}\left(\rho\frac{\partial\xi}{\partial\rho}\right). \tag{C.6}$$

Rewriting then eqn (C.6) in dimensionless form we have

$$\dot{\bar{\xi}} = \frac{D\xi_L}{\bar{\rho}}\frac{\partial}{\partial\bar{\rho}}\left(\bar{\rho}\frac{\partial\bar{\xi}}{\partial\bar{\rho}}\right). \tag{C.7}$$

Moreover, by imposing the conservation of cell receptors, we get

$$\begin{aligned} 0 &= \frac{\partial}{\partial t}\left(\frac{1-p}{\alpha_p}\bar{A}_w + 2\pi\int_{\bar{\rho}_0}^{\infty}\bar{\xi}\bar{\rho}\,\mathrm{d}\bar{\rho}\right) \\ &= \frac{1-p}{\alpha_p}\dot{\bar{A}}_w - 2\pi\bar{\rho}_0\dot{\bar{\rho}}_0\bar{\xi}_+ + 2\pi\int_{\bar{\rho}_0}^{\infty}\dot{\bar{\xi}}\bar{\rho}\,\mathrm{d}\bar{\rho} \\ &= \frac{1-p}{\alpha_p}\dot{\bar{A}}_w - 2\pi\bar{\rho}_0\dot{\bar{\rho}}_0\bar{\xi}_+ + 2\pi D\xi_L\int_{\bar{\rho}_0}^{\infty}\frac{\partial}{\partial\bar{\rho}}\left(\bar{\rho}\frac{\partial\bar{\xi}}{\partial\bar{\rho}}\right)\mathrm{d}\bar{\rho} \end{aligned} \tag{C.8}$$

whence

$$D\xi_L\bar{\xi}_+' = \frac{1-p}{2\pi\bar{\rho}_0\alpha_p}\dot{\bar{A}}_w - \dot{\bar{\rho}}_0\bar{\xi}_+ \tag{C.9}$$

where $\bar{\xi}_+ := \lim_{\bar{\rho}\to\bar{\rho}_0^+}\bar{\xi}$ and $\bar{\xi}_+' := \lim_{\bar{\rho}\to\bar{\rho}_0^+}\frac{\partial\bar{\xi}}{\partial\bar{\rho}}$ are the limit values of the cell receptor density and its radial derivative at the front of the wrapping region, respectively.

Finally, by taking the time derivative of the free energy (C.2), plugging in eqn (C.7), integrating by parts, and exploiting eqn (C.9) together with the time derivative of eqn (C.5) and the approximation $\Delta\bar{A} \approx \bar{A}_w - \pi\bar{\rho}_0{}^2$, we arrive at

$$\begin{aligned} \mathscr{E} = &-\dot{\bar{A}}_w\Bigg\{\frac{1-p}{\alpha_p}\left(1+\ln\frac{\bar{\xi}_+}{\bar{\xi}_0}+\ln\frac{\alpha_p\bar{\xi}_0}{1-p}\right) - \frac{1}{\alpha_p}\left(1-\frac{\bar{A}_w}{2\pi\bar{R}^2\alpha_p}\right)\bar{\xi}_+ \\ &+\frac{1-p}{\alpha_p}\bar{e}_{RL} + \bar{\xi}_c\bar{e}_c - \left(1-\frac{p}{\alpha_p}\bar{A}_p\right)\frac{1}{\bar{R}^2}\left[2\bar{\kappa}_m + 2\bar{\kappa}_c\left(1-\frac{\bar{R}}{\bar{R}^\star}\right)^2 + \bar{\bar{\kappa}}_c\right] \\ &-\frac{p}{\alpha_p}\int_{\mathscr{S}_p}\left[2\bar{\kappa}_m\bar{H}^2 + 2\bar{\kappa}_c(\bar{H}-\bar{H}^\star)^2 + \bar{\bar{\kappa}}_c\bar{K}\right]\mathrm{d}\bar{A} \\ &-\bar{\sigma}\left[1-\frac{1}{\alpha_p}\left(1-\frac{\bar{A}_w}{2\pi\bar{R}^2\alpha_p}\right)\right]\Bigg\} - 2\pi D\xi_L\int_{\bar{\rho}_0(t)}^{+\infty}\bar{\xi}\left(\frac{\partial\ln\bar{\xi}}{\partial\bar{\rho}}\right)^2\bar{\rho}\,\mathrm{d}\bar{\rho} \end{aligned} \tag{C.10}$$

where the last integral term represents the rate of energy consumed during receptor transport.[51] By assuming that the rate of the free energy reduction is greater than that of energy dissipation, due to receptor transport, we derive the inequality

$$\begin{aligned} &(1-p)\bar{e}_{RL} + \alpha_p\bar{\xi}_c\bar{e}_c + (1-p)\left(1+\ln\frac{\bar{\xi}_+}{\bar{\xi}_0}+\ln\frac{\alpha_p\bar{\xi}_0}{1-p}\right) \\ &\quad -\left(1-\frac{\bar{A}_w}{2\pi\bar{R}^2\alpha_p}\right)\bar{\xi}_+ > \left(\alpha_p - p\bar{A}_p\right) \\ &\frac{1}{\bar{R}^2}\left[2\bar{\kappa}_m + 2\bar{\kappa}_c\left(1-\frac{\bar{R}}{\bar{R}^\star}\right)^2 + \bar{\bar{\kappa}}_c\right] \\ &\quad + p\int_{\mathscr{S}_p}\left[2\bar{\kappa}_m\bar{H}^2 + 2\bar{\kappa}_c(\bar{H}-\bar{H}^\star)^2 + \bar{\bar{\kappa}}_c\bar{K}\right]\mathrm{d}\bar{A} \\ &\quad + \bar{\sigma}\left[\alpha_p - \left(1-\frac{\bar{A}_w}{2\pi\bar{R}^2\alpha_p}\right)\right]. \end{aligned} \tag{C.11}$$

Finally, by approximating $\bar{\xi}_+ \approx \bar{\xi}_0$ and $\bar{A}_w \approx 2\pi\bar{R}^2(1-\cos\beta_w)\alpha_p$, we get

$$\begin{aligned} &(1-p)\bar{e}_{RL} + \alpha_p\bar{\xi}_c\bar{e}_c + (1-p)\left(1+\ln\frac{\alpha_p\bar{\xi}_0}{1-p}\right) - \cos\beta_w\bar{\xi}_0 \\ &\quad > (1-p/p_{max})\left[2\bar{\kappa}_m + 2\bar{\kappa}_c(1-\bar{R}/\bar{R}^\star)^2 + \bar{\bar{\kappa}}_c\right]\frac{1}{\bar{R}^2} \\ &\quad + p\int_{\mathscr{S}_p}\left[2\bar{\kappa}_m\bar{H}^2 + 2\bar{\kappa}_c(\bar{H}-\bar{H}^\star)^2 + \bar{\bar{\kappa}}_c K\right]\mathrm{d}\bar{A} + \left(\alpha_p - \cos\beta_w\right)\bar{\sigma}. \end{aligned} \tag{C.12}$$

eqn (8) follows by setting $\beta_w = 0$ in eqn (C.12), and it reduces to eqn (7) for $p = 0$.

D Emergence of a maximum radius for the particle uptake

For the clathrin-dependent pathway, a maximum radius might derive from eqn (7), which provides a necessary condition for initiating wrapping of a spherical particle. In this section we determine the critical thresholds for the appearance of such a maximum radius, in terms of bending rigidity and spontaneous curvature of the clathrin coat.

Eqn (7) is a quadratic inequality in the dimensionless radius $\bar{R}$, namely,

$$a\bar{R}^2 + b\bar{R} - c > 0 \tag{D.1}$$

where $a := \bar{e}_{\mathrm{RL}} + \bar{\xi}_{\mathrm{c}}\bar{e}_{\mathrm{c}} + 1 - \bar{\xi}_0 + \ln\bar{\xi}_0 - 2\bar{\kappa}_{\mathrm{c}}/\bar{R}^{\star^2}$, $b := 4\bar{\kappa}_{\mathrm{c}}/\bar{R}^{\star}$, and $c := 2(\bar{\kappa}_{\mathrm{m}} + \bar{\kappa}_{\mathrm{c}}) + \bar{\tilde{\kappa}}_{\mathrm{c}}$. Thus, the presence of a protein coat with a spontaneous curvature can determine a maximum value $\bar{R}_{\max}$ for the particle radius if $a < 0$.

For a fixed bending rigidity $\bar{\kappa}_{\mathrm{c}}$, this condition holds if the spontaneous radius of curvature satisfies

$$\bar{R}^{\star} < \bar{R}_0^{\star} := \sqrt{\frac{2\bar{\kappa}_{\mathrm{c}}}{\bar{e}_{\mathrm{RL}} + \bar{\xi}_{\mathrm{c}}\bar{e}_{\mathrm{c}} + 1 - \bar{\xi}_0 + \ln\bar{\xi}_0}}. \tag{D.2}$$

In passing, we notice that we implicitly assumed that $\bar{e}_{\mathrm{RL}} + \bar{\xi}_{\mathrm{c}}\bar{e}_{\mathrm{c}} + 1 - \bar{\xi}_0 > -\ln\bar{\xi}_0$, otherwise the binding energy would be insufficient to drive the wrapping.

Analogously, for any fixed spontaneous radius of curvature $\bar{R}^{\star}$, we can derive the critical value of the bending rigidity as

$$\bar{\kappa}_{\mathrm{c}} > \bar{\kappa}_{\mathrm{c},0} := \frac{\bar{R}^{\star^2}}{2}\left(\bar{e}_{\mathrm{RL}} + \bar{\xi}_{\mathrm{c}}\bar{e}_{\mathrm{c}} + 1 - \bar{\xi}_0 + \ln\bar{\xi}_0\right). \tag{D.3}$$

E The obstacle problem

We determine the configuration of the membrane in a region associated with a protrusion, $\mathscr{S}_{\mathrm{p}}$, as solution to the obstacle problem (*i.e.* the minimization of the free energy of the membrane within the limits of compatibility)

$$\min_{\bar{h}\in\mathscr{K}} \int_{\mathscr{S}_{\mathrm{p}}} \left[2\bar{\kappa}_{\mathrm{m}}\bar{H}^2 + 2\bar{\kappa}_{\mathrm{c}}(\bar{H} - \bar{H}^{\star})^2 + \bar{\sigma}\right] \mathrm{d}\bar{A} \tag{E.1}$$

where $\mathscr{K}$ is the set of all admissible configurations for the cell membrane wrapping the inhibitor and being clamped to the particle at the boundary $\partial\mathscr{S}_{\mathrm{p}}$. In eqn (E.1) we dropped the saddle-splay term of the protein coat because the prescribed boundary conditions force the geodesic curvature at the boundary so that integral of the Gaussian curvature amounts to a constant, in view of the Gauss-Bonnet theorem.

We adopt the Monge parametrization to describe both the membrane and the obstacle and, by assuming axial symmetry of the problem, we introduce the corresponding dimensionless heights $\bar{h}(\bar{\rho})$ and $\bar{h}_0(\bar{\rho})$ as functions of the dimensionless polar coordinate $\bar{\rho}$. Thus, the problem reads as

$$\min_{\bar{h}\in\mathscr{K}} \int_0^{\bar{R}\sin(1/\bar{R})} \left(2\bar{H}^2 - \frac{4\bar{\kappa}_{\mathrm{c}}\bar{H}^{\star}}{\bar{\kappa}_{\mathrm{m}} + \bar{\kappa}_{\mathrm{c}}}\bar{H} + \frac{2\bar{\kappa}_{\mathrm{c}}\bar{H}^{\star^2} + \bar{\sigma}}{\bar{\kappa}_{\mathrm{m}} + \bar{\kappa}_{\mathrm{c}}}\right)\bar{\rho}\sqrt{1 + \bar{h}'^2}\,\mathrm{d}\bar{\rho} \tag{E.2}$$

with the membrane configuration $\bar{h}$ belonging to the set of sufficiently regular height functions that fulfill the compatibility constraints, *i.e.*,

$$\bar{\mathscr{H}} := \left\{ v: \begin{array}{ll} v \geq \bar{h}_0 & \text{for } 0 \leq \rho \leq \bar{R}\sin(1/\bar{R}) \\ v = \bar{h}_0 & \text{at } \bar{\rho} = \bar{R}\sin(1/\bar{R}) \\ v' = \bar{h}_0' & \text{at } \bar{\rho} = \bar{R}\sin(1/\bar{R}) \\ v' = v''' = 0 & \text{at } \bar{\rho} = 0 \end{array} \right\} \tag{E.3}$$

where primes denote differentiation with respect to $\bar{\rho}$. In particular, we define the obstacle as

$$\bar{h}_0(\bar{\rho}) = \max\{\bar{h}_{\mathrm{p}}, \bar{h}_{\mathrm{i}}\} \tag{E.4}$$

where $\bar{h}_{\mathrm{p}}$ is the height function of the particle, and $\bar{h}_{\mathrm{i}}$ is the height function of the inhibitor, namely

$$\bar{h}_{\mathrm{p}} := \sqrt{\bar{R}^2 - \bar{\rho}^2} - \bar{R}\cos\frac{1}{\bar{R}} \tag{E.5}$$

and

$$\bar{h}_i := \begin{cases} \sqrt{\bar{r}^2 - \bar{\rho}^2} - \bar{r} + \bar{\delta} + \bar{R}\left(1 - \cos\frac{1}{\bar{R}}\right) & \text{if } \bar{\rho}^2 \leq \bar{r}^2 \\ 0 & \text{if } \bar{\rho}^2 > \bar{r}^2 \end{cases} \tag{E.6}$$

where $\bar{r} := r\sqrt{\xi_{\mathrm{L}}}$ is the dimensionless radius of the spherical protrusion and $\bar{\delta} := \delta\sqrt{\xi_{\mathrm{L}}}$ is the dimensionless indentation $\delta = 2dr$ (see Fig. 3).

In terms of the adopted parametrization, the mean curvature of the membrane having height $\bar{h}(\bar{\rho})$ is given by

$$\bar{H}(\bar{\rho}) = \frac{\bar{\rho}\bar{h}'' + \bar{h}'\left(1 + \bar{h}'^2\right)}{2\bar{\rho}\left(1 + \bar{h}'^2\right)^{3/2}}. \tag{E.7}$$

The obstacle problem (E.2)–(E.4) depends only on the three dimensionless parameters that define the specific geometry of the obstacle, *i.e.*, $\bar{r}$, $\bar{\delta}$, and $\bar{R}$, and the two dimensionless parameters $4\bar{\kappa}_{\mathrm{c}}\bar{H}^{\star}/(\bar{\kappa}_{\mathrm{m}} + \bar{\kappa}_{\mathrm{c}})$ and $\left(2\bar{\kappa}_{\mathrm{c}}\bar{H}^{\star^2} + \bar{\sigma}\right)/(\bar{\kappa}_{\mathrm{m}} + \bar{\kappa}_{\mathrm{c}})$. This problem is a variational inequality and we solve it numerically by using the penalty method (*e.g.*, see ref. 60 and references therein), namely, we minimize the penalized functional

$$\int_0^{\bar{R}\sin(1/\bar{R})} \left(2\bar{H}^2 - \frac{4\bar{\kappa}_{\mathrm{c}}\bar{H}^{\star}}{\bar{\kappa}_{\mathrm{m}} + \bar{\kappa}_{\mathrm{c}}}\bar{H} + \frac{2\bar{\kappa}_{\mathrm{c}}\bar{H}^{\star^2} + \bar{\sigma}}{\bar{\kappa}_{\mathrm{m}} + \bar{\kappa}_{\mathrm{c}}}\right)\bar{\rho}\sqrt{1 + \bar{h}'^2}\,\mathrm{d}\bar{\rho} + \frac{P}{2}\int_0^{\bar{R}\sin(1/\bar{R})} \left[\left(\bar{h} - \bar{h}_0\right)_-\right]^2 \bar{\rho}\,\mathrm{d}\bar{\rho} \tag{E.8}$$

where $(\cdot)_- := \min\{0, \cdot\}$ is the "negative part" function and $P \gg 1$ is the penalty parameter.

We derive the weak form of the problem as a system of the two following variational equations, *i.e.*,

$$0 = \int_0^{\bar{R}\sin(1/\bar{R})} \frac{\tilde{h}'}{1 + \bar{h}'^2}\left[\left(3\bar{H}^2 + \frac{2\bar{\kappa}_{\mathrm{c}}\bar{H}^{\star^2} + \bar{\sigma}}{\bar{\kappa}_{\mathrm{m}} + \bar{\kappa}_{\mathrm{c}}}\right)\bar{\rho}\bar{h}'\sqrt{1 + \bar{h}'^2} - 2\bar{\rho}\bar{H}' + 2\left(\bar{H} - \frac{\bar{\kappa}_{\mathrm{c}}\bar{H}^{\star}}{\bar{\kappa}_{\mathrm{m}} + \bar{\kappa}_{\mathrm{c}}}\right)\bar{h}'^2\right]\mathrm{d}\bar{\rho} + P\int_0^{\bar{R}\sin(1/\bar{R})} \tilde{h}\left(\bar{h} - \bar{h}_0\right)_-\bar{\rho}\,\mathrm{d}\bar{\rho} \tag{E.9}$$

$$0 = \int_0^{\bar{R}\sin(1/\bar{R})} \tilde{H}\left(2\bar{H} - \frac{\bar{h}'}{\bar{\rho}\sqrt{1+\bar{h}'^2}}\right) \mathrm{d}\bar{\rho} + \int_0^{\bar{R}\sin(1/\bar{R})} \tilde{H}' \frac{\bar{h}'}{\sqrt{1+\bar{h}'^2}} \mathrm{d}\bar{\rho} - \tilde{H}\frac{\bar{h}'}{\sqrt{1+\bar{h}'^2}}\Bigg|_0^{\bar{R}\sin(1/\bar{R})} \tag{E.10}$$

where $\tilde{h}$ and $\tilde{H}$ are the test functions.

We implemented and solved the weak formulation (E.9) and (E.10) *via* finite element analysis based on the FEniCS Project Version 2019.1.0.[59] For our numerical simulations we used a penalty parameter $P = 10^8$. The Python code is available at https://github.com/daniele-agostinelli/ObstacleProblem.git.

F Single-spaced and double-spaced configurations

Throughout this study we assumed that the cellular membrane wrapping around an inhibitor binds to the closest active ligands located at distance ℓ from the inhibitor (single-spaced configuration). However, other configurations might be more energetically convenient, for example one in which the membrane binds to active ligands located at a distance 2ℓ (double-spaced configuration). If each inhibitor is associated with an area corresponding to n times the angle ℓ/R, there are at most $\sim 2/(1-\cos(n/\bar{R}))$ inhibitors. By comparing this number with $4\pi\bar{R}^2 p$, we get the relationship

$$p = \frac{1}{2\pi\bar{R}^2[1-\cos(n/\bar{R})]} \approx \frac{1}{\pi n^2} \tag{F.1}$$

where the last approximation holds for $\bar{R} \gg 1$ (large particle or high ligand density).

From the estimate (F.1), a configuration with a doubled angle (double-spaced) is possible for $p < 0.08$. In this case we can compare the energies of the single-spaced ($n = 1$) and double-spaced ($n = 2$) configurations shown in Fig. 8. The latter is convenient if

$$\Delta(\mathscr{E}_{\mathrm{el}} + \mathscr{E}_{\mathrm{ad}}) = \left(\mathscr{E}_{\mathrm{el}}^{(2)} - \mathscr{E}_{\mathrm{el}}^{(1)}\right) + \left(\mathscr{E}_{\mathrm{ad}}^{(2)} - \mathscr{E}_{\mathrm{ad}}^{(1)}\right) \leq 0 \tag{F.2}$$

with $^{(1)}$ indicating single-spaced configuration and $^{(2)}$ double-spaced.

Fig. 9 shows the domains of the two configurations in the parameter space ($\bar{r}$, $\bar{R}$), for selected values of the model parameters. Fig. 9a reports the case of receptor-mediated endocytosis, in the absence of protein coats, while Fig. 9b reports the case of protein coat. In the latter case, compared to the former, we observe higher sensitivity to $\bar{R}$, while receptor density $\bar{\varepsilon}_0$ is less influential.

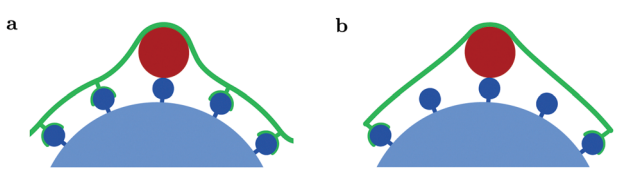

Fig. 8 Two-dimensional illustration of the (a) single-space (n = 1) and (b) double-spaced (n = 2) configurations. For a low fraction of inhibited ligands, $p \sim 0.1$, the former might be energetically more expensive than the latter, where cell receptors do not bind to the ligands that are proximal to the protrusion.

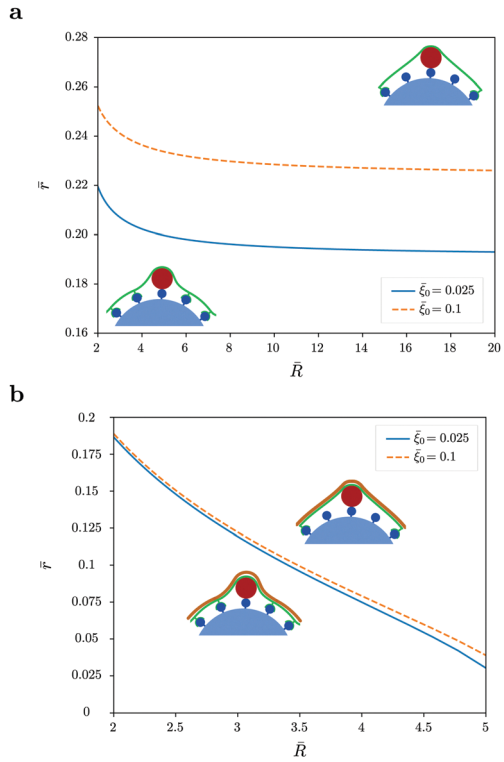

Fig. 9 Comparison between the energetic cost of single-spaced and double-spaced configurations: larger protrusions (increasing $\bar{r}$) leads to higher bending cost, which might (not) be compensated by the enthalpic gain due to receptor–ligand bindings, thus resulting in a critical threshold of the inhibitor size, $\bar{r}$. The parameter space ($\bar{R}$, $\bar{r}$) is split into regions where one configuration is more convenient than the other one, as indicated in the plots ($\bar{r}$ above the line provides double-spaced). We report the boundaries of these regions for different values of the ratio between receptors and ligands, $\bar{\xi}_0 := \xi_0/\xi_L$, for the case of (a) receptor-mediated endocytosis without any protein coat ($\bar{\kappa}_c = \bar{\tilde{\kappa}}_c = \bar{H}^\star = \bar{e}_c = 0$) and (b) clathrin-mediated endocytosis for $\bar{H}^\star \approx -0.28$, $\bar{\kappa}_c = 300$, $\bar{\tilde{\kappa}}_c = 0$, $\bar{e}_c = 23$. We set $d = 1$ and other model parameters as $\bar{e}_{RL} = 15$, $\bar{\sigma} = 1$, $\xi_L = 5 \times 10^{-3}$ nm^{-2}, $p \approx 0.08$.

G The effect of inhibiting ligands without protrusions

In this appendix we examine the effect of inhibiting particle ligands without protrusions ($p > 0$ and $\bar{r} = 0$). In this case eqn (8) yields

$$\bar{\tilde{\xi}}_c\bar{e}_c + (1-p)\left(\bar{e}_{RL} + 1 + \ln\frac{\bar{\tilde{\xi}}_0}{1-p}\right) - \bar{\tilde{\xi}}_0 > \left[2\bar{\kappa}_m + 2\bar{\kappa}_c(1-\bar{R}/\bar{R}^\star)^2 + \bar{\tilde{\kappa}}_c\right]\frac{1}{\bar{R}^2}. \tag{G.1}$$

By assuming that $\bar{\tilde{\xi}}_c\bar{e}_c + (1-p)[\bar{e}_{RL} + 1 + \ln(\bar{\tilde{\xi}}_0/(1-p))] > \bar{\tilde{\xi}}_0$, the presence of clathrin provides both a minimum and a maximum value for the particle radius if the spontaneous radius of

curvature satisfies

$$\bar{R}^{\star} < \sqrt{\frac{2\bar{\kappa}_{\mathrm{c}}}{\bar{\xi}_{\mathrm{c}}\bar{e}_{\mathrm{c}} + (1-p)\left(\bar{e}_{\mathrm{RL}} + 1 + \ln\frac{\bar{\xi}_0}{1-p}\right) - \bar{\xi}_0}}. \tag{G.2}$$

If clathrin is absent or the spontaneous radius of curvature is above such a threshold, there exists only a minimum particle radius. In particular, in the absence of clathrin, we get

$$\bar{R}_{\min} = \sqrt{\frac{2\bar{\kappa}_{\mathrm{m}}}{(1-p)\left(\bar{e}_{\mathrm{RL}} + 1 + \ln\frac{\bar{\xi}_0}{1-p}\right) - \bar{\xi}_0}}. \tag{G.3}$$

Since $(1-p)\left(\bar{e}_{\mathrm{RL}} + 1 + \ln\frac{\bar{\xi}_0}{1-p}\right) \to 0^+$ for $p \to 1^-$, the denominator vanishes at $p = p^{\star}$ where $p^{\star} < 1$. More precisely, for the relevant parameter values,

$$p^{\star} = 1 + \frac{\bar{\xi}_0}{W_{-1}\left(-\mathrm{e}^{-1-\bar{e}_{\mathrm{RL}}}\right)} \tag{G.4}$$

where $W_k(\cdot)$ denotes the kth branch of the Lambert W-Function. Then $\bar{R}_{\min} \to +\infty$ for $p \to p^{\star -}$. We observe that the critical fraction $p^{\star}(\bar{r} = 0)$ is above 97% for the parameters used in this study, and $\bar{e}_{\mathrm{RL}} > \bar{\xi}_0 - 1 - \ln\bar{\xi}_0$, which is the minimum receptor–ligand binding energy for having sufficient driving force. This implies that, in the absence of clathrin, inhibiting ligands without additional bending penalty is an inefficient method of blocking the wrapping, since almost all ligands should be inhibited.

Acknowledgements

The authors gratefully acknowledge the useful discussions with Dr Don Sin (Saint Paul Hospital) and Masahiro Niikura (Simon Fraser University). M. B. and G. J. E. acknowledge the financial support from the New Frontiers in Research Funds – Exploration (NFRFE-2018-00730); M. B. acknowledges the financial support from the Natural Sciences and Engineering Research Council of Canada (NSERC) (RGPIN-2017-04464, and ALLRP554607-20); D. A. acknowledges the financial support from the Michael Smith Foundation for Health Research (RT-2021-1954).

References

1 S. Zhang, H. Gao and G. Bao, *ACS Nano*, 2015, **9**, 8655–8671.
2 S. Behzadi, V. Serpooshan, W. Tao, M. Hamaly, M. Alkawareek, E. Dreaden, D. Brown, A. Alkilany, O. Farokhzad and M. Mahmoudi, *Chem. Soc. Rev.*, 2017, **46**, 4218–4244.
3 R. Mashl and R. Bruinsma, *Biophys. J.*, 1998, **74**, 2862–2875.
4 S. Gratton, P. Ropp, P. Pohlhaus, J. Luft, V. Madden, M. Napier and J. DeSimone, *Proc. Natl. Acad. Sci. U. S. A.*, 2008, **105**, 11613–11618.
5 R. Petros and J. DeSimone, *Nat. Rev. Drug Discovery*, 2010, **9**, 615–627.
6 K. Kettler, K. Veltman, D. van de Meent, A. van Wezel and A. Hendriks, *Environ. Toxicol. Chem.*, 2014, **33**, 481–492.
7 T. Sun, Y. Zhang, B. Pang, D. Hyun, M. Yang and Y. Xia, *Angew. Chem., Int. Ed.*, 2014, **53**, 12320–12364.
8 S. Patel, J. Kim, M. Herrera, A. Mukherjee, A. Kabanov and G. Sahay, *Adv. Drug Delivery Rev.*, 2019, **144**, 90–111.
9 Y. Hui, X. Yi, F. Hou, D. Wibowo, F. Zhang, D. Zhao, H. Gao and C.-X. Zhao, *ACS Nano*, 2019, **13**, 7410–7424.
10 A. Albanese, P. Tang and W. Chan, *Annu. Rev. Biomed. Eng.*, 2012, **14**, 1–16.
11 I. Canton and G. Battaglia, *Chem. Soc. Rev.*, 2012, **41**, 2718–2739.
12 L. Shang, K. Nienhaus and G. Nienhaus, *J. Nanobiotechnol.*, 2014, **12**, 1–11.
13 H. Gao, W. Shi and L. Freund, *Proc. Natl. Acad. Sci. U. S. A.*, 2005, **102**, 9469–9474.
14 A. Chaudhuri, G. Battaglia and R. Golestanian, *Phys. Biol.*, 2011, **8**, 046002.
15 P. Decuzzi and M. Ferrari, *Biomaterials*, 2007, **28**, 2915–2922.
16 F. Osaki, T. Kanamori, S. Sando, T. Sera and Y. Aoyama, *J. Am. Chem. Soc.*, 2004, **126**, 6520–6521.
17 B. Chithrani, A. Ghazani and W. Chan, *Nano Lett.*, 2006, **6**, 662–668.
18 W. Jiang, B. Kim, J. Rutka and W. Chan, *Nat. Nanotechnol.*, 2008, **3**, 145–150.
19 K. Shapero, F. Fenaroli, I. Lynch, D. Cottell, A. Salvati and K. Dawson, *Mol. BioSyst.*, 2011, **7**, 371–378.
20 J. Rejman, V. Oberle, I. Zuhorn and D. Hoekstra, *Biochem. J.*, 2004, **377**, 159–169.
21 B. Chithrani and W. Chan, *Nano Lett.*, 2007, **7**, 1542–1550.
22 J.-M. Oh, S.-J. Choi, G.-E. Lee, J.-E. Kim and J.-H. Choy, *Chem. – Asian J.*, 2009, **4**, 67–73.
23 J. Zhu, L. Liao, L. Zhu, P. Zhang, K. Guo, J. Kong, C. Ji and B. Liu, *Talanta*, 2013, **107**, 408–415.
24 M. Marsh and A. Helenius, *Cell*, 2006, **124**, 729–740.
25 J. Flint, V. Racaniello, G. Rall, A. Skalka and L. Enquist, *Principles of virology, Volume 1: Molecular biology*, ASM Press, 4th edn, 2015.
26 P. Decuzzi and M. Ferrari, *Biophys. J.*, 2008, **94**, 3790–3797.
27 X. Yi, X. Shi and H. Gao, *Nano Lett.*, 2014, **14**, 1049–1055.
28 Z. Shen, H. Ye, X. Yi and Y. Li, *ACS Nano*, 2019, **13**, 215–228.
29 H. Jin, D. Heller, R. Sharma and M. Strano, *ACS Nano*, 2009, **3**, 149–158.
30 X. Yi and H. Gao, *Nanoscale*, 2017, **9**, 454–463.
31 X. Banquy, F. Suarez, A. Argaw, J.-M. Rabanel, P. Grutter, J.-F. Bouchard, P. Hildgen and S. Giasson, *Soft Matter*, 2009, **5**, 3984–3991.
32 A. Verma and F. Stellacci, *Small*, 2010, **6**, 12–21.
33 J. Forster, J. Krausser, M. Vuyyuru, B. Baum and A. Šarić, *Phys. Rev. Lett.*, 2020, **125**, 228101.
34 D. Lauster, S. Klenk, K. Ludwig, S. Nojoumi, S. Behren, L. Adam, M. Stadtmüller, S. Saenger, S. Zimmler and K. Hönzke, *et al.*, *Nat. Nanotechnol.*, 2020, **15**, 373–379.
35 B. Lewis and D. Engelman, *J. Mol. Biol.*, 1983, **166**, 211–217.
36 P. Canham, *J. Theor. Biol.*, 1970, **26**, 61–81.

37 W. Helfrich, *Zeitschrift für Naturforschung C*, 1973, **28**, 693–703.
38 O. Avinoam, M. Schorb, C. Beese, J. Briggs and M. Kaksonen, *Science*, 2015, **348**, 1369–1372.
39 D. Bucher, F. Frey, K. Sochacki, S. Kummer, J.-P. Bergeest, W. Godinez, H.-G. Kräusslich, K. Rohr, J. Taraska, U. Schwarz and S. Boulant, *Nat. Commun.*, 2018, **9**, 1–13.
40 F. Frey, PhD thesis, University of Heidelberg, 2019.
41 K. Sochacki, B. Heine, G. Haber, J. Jimah, B. Prasai, M. Alfonzo-Méndez, A. Roberts, A. Somasundaram, J. Hinshaw and J. Taraska, *Dev. Cell*, 2021, **56**, 1131–1146.e3.
42 J. Hassinger, G. Oster, D. Drubin and P. Rangamani, *Proc. Natl. Acad. Sci. U. S. A.*, 2017, **114**, E1118–E1127.
43 M. Mund, A. Tschanz, Y.-L. Wu, F. Frey, J. Mehl, M. Kaksonen, O. Avinoam, U. Schwarz and J. Ries, *Super-resolution microscopy reveals partial preassembly and subsequent bending of the clathrin coat during endocytosis*, 2022, **https://www.biorxiv.org/content/early/2022/01/11/2021.10.12.463947**.
44 K. Sochacki, A. Dickey, M.-P. Strub and J. Taraska, *Nat. Cell Biol.*, 2017, **19**, 352–361.
45 F. Frey and U. S. Schwarz, *Soft Matter*, 2020, **16**, 10723–10733.
46 M. Stoeber, P. Schellenberger, C. Siebert, C. Leyrat, A. Helenius and K. Grünewald, *Proc. Natl. Acad. Sci. U. S. A.*, 2016, **113**, E8069–E8078.
47 G. Vigers, R. Crowther and B. Pearse, *EMBO J.*, 1986, **5**, 2079–2085.
48 J. Pedersen, *Eur. Biophys. J.*, 1993, **22**, 79–95.
49 M. Saleem, S. Morlot, A. Hohendahl, J. Manzi, M. Lenz and A. Roux, *Nat. Commun.*, 2015, **6**, 1–10.
50 M. Deserno, *Phys. Rev. E: Stat., Nonlinear, Soft Matter Phys.*, 2004, **69**, 031903.
51 L. Freund and Y. Lin, *J. Mech. Phys. Solids*, 2004, **52**, 2455–2472.
52 D. Steigmann, *The role of mechanics in the study of lipid bilayers*, Springer, Cham, 2017, vol. 577.
53 A. Banerjee, A. Berezhkovskii and R. Nossal, *Biophys. J.*, 2012, **102**, 2725–2730.
54 R. Nossal, *Traffic*, 2001, **2**, 138–147.
55 A. Jin, K. Prasad, P. Smith, E. Lafer and R. Nossal, *Biophys. J.*, 2006, **90**, 3333–3344.
56 G. Kumar and A. Sain, *Phys. Rev. E*, 2016, **94**, 062404.
57 J. Heuser, *J. Cell Biol.*, 1980, **84**, 560–583.
58 L. Traub, *PLoS Biol.*, 2011, **9**, 1–5.
59 A. Logg, K.-A. Mardal and G. Wells, *Automated solution of differential equations by the finite element method: The FEniCS book*, Springer Berlin Heidelberg, Berlin, Heidelberg, 2012, vol. 84.
60 R. Glowinski, *Generalities on Elliptic Variational Inequalities and on Their Approximation*, Springer Berlin Heidelberg, Berlin, Heidelberg, 1984, pp. 1–26.
61 J. Blechinger, A. Bauer, A. Torrano, C. Gorzelanny, C. Bräuchle and S. Schneider, *Small*, 2013, **9**, 3970–3980.
62 M. Arroyo and A. DeSimone, *Phys. Rev. E: Stat., Nonlinear, Soft Matter Phys.*, 2009, **79**, 031915.
63 X. Yi and H. Gao, *Langmuir*, 2016, **32**, 13252–13260.
64 T. Auth and G. Gompper, *Phys. Rev. E: Stat., Nonlinear, Soft Matter Phys.*, 2009, **80**, 031901.
65 N. Walani, J. Torres and A. Agrawal, *Proc. Natl. Acad. Sci. U. S. A.*, 2015, **112**, E1423–E1432.
66 A. Collins, A. Warrington, K. A. Taylor and T. Svitkina, *Curr. Biol.*, 2011, **21**, 1167–1175.
67 M. Mettlen, P.-H. Chen, S. Srinivasan, G. Danuser and S. Schmid, *Annu. Rev. Biochem.*, 2018, **87**, 871–896.
68 M. Kaksonen and A. Roux, *Nat. Rev. Mol. Cell Biol.*, 2018, **19**, 313–326.
69 S. Boulant, C. Kural, J.-C. Zeeh, F. Ubelmann and T. Kirchhausen, *Nat. Cell Biol.*, 2011, **13**, 1124–1131.
70 S. Tzlil, M. Deserno, W. Gelbart and A. Ben-Shaul, *Biophys. J.*, 2004, **86**, 2037–2048.